SOLAR SUSTAINED PLASMA/ABSORBER CONCEPTUAL DESIGN

By

Richard J. Rodgers

Nicholas L. Krascella

John S. Kendall

February 1979

Prepared under Contract No. NAS2-10010

By

UNITED TECHNOLOGIES RESEARCH CENTER

East Hartford, Ct.

for

AMES RESEARCH CENTER

National Aeronautics and Space Administration

NASA CR-152304

UNITED TECHNOLOGIES RESEARCH CENTER

UNITED TECHNOLOGIES

East Hartford, Connecticut 06108

Report R79-914392

Solar Sustained Plasma/Absorber Conceptual Design

FINAL REPORT
1 August 1978 Through 28 February 1979
Contract NAS2-10010

UNCLASSIFIED

REPORTED BY R. J. Rodgers

N. L. Krascella

J. S. Kendall

APPROVED BY M. Suo

DATE February 28, 1979

NO. OF PAGES _____ COPY NO. _____

Report R79-914392

Solar Sustained Plasma/Absorber Conceptual Design

FINAL REPORT
1 August 1978 Through 28 February 1979
Contract NAS2-10010

TABLE OF CONTENTS

Report R79-914392

Solar Sustained Plasma/Absorber Conceptual Design

Final Report
1 August 1978 Through 28 February 1979
Contract NAS2-10010

SUMMARY

An analytic study was performed to evaluate a space power system concept which uses concentrated solar energy to heat a working fluid to temperatures as high as 4000 K. The high temperature working fluid could be used for efficient electric power production in advanced thermal or magnetohydrodynamic conversion cycles. Energy absorber configurations utilizing carbon particles or cesium vapor absorber material were investigated. Results of detailed radiant heat transfer calculations indicated approximately 86 percent of the incident solar energy could be absorbed within a 12-cm-dia flowing stream of gas borne carbon particles. Calculated total energy absorption in the cesium vapor seeded absorber configuration ranged from 34 percent to 64 percent of the incident solar energy. Solar flux concentration ratios of between approximately 3000 and 10,000 will be required to sustain absorber temperatures in the range from 3000 K to 4000 K.

A reference power system sized to produce an output power of 100 kWe was evaluated. The result yielded a Brayton cycle efficiency of 41 percent corresponding to an absorber working fluid temperature of 3000 K, heat rejection temperatures of 700 K, and total system pressure of 10 atm. Higher efficiencies would be achieved with increases in absorber working fluid temperature or with decreases in the heat rejection temperature. Estimated total system masses for the reference system are 3510 kg based on state-of-the-art components and 2420 kg based on advanced state-of-the-art component development. Corresponding values of specific power are 28 W/kg and 41 W/kg, respectively. Significant increases in specific power appear possible through development of lighter weight optical components and advanced radiator concepts.

A series of proof-of-principle experiments are required to demonstrate the technical feasibility of the solar absorber concept and to provide a performance data base which may be used for more accurate system assessments.

RESULTS AND CONCLUSIONS

1. A reference solar absorber configuration with the following principal characteristics was selected: (a) absorber region diameter of approximately 12 cm, (b) argon buffer gas is used to provide fluid mechanical confinement of gas borne carbon particles within a coflowing stream, (c) power incident on absorber region equal to 268 kW, (d) image plane flux intensity equal to 2.335 kW/cm^2, (e) bulk exit temperature of absorber region equal to 3000 K, and (f) total pressure equal to 10 atm.

2. The calculated performance of the reference Brayton power system configuration for a 100 kWe output power was: (a) energy exchanger inlet temperature equal to 3000 K, (b) turbine inlet temperature equal to 1200 K, (c) heat rejection temperature equal to 700 K, (d) cycle pressure ratio equal to 4, (e) cycle efficiency equal to 41 percent. Initial estimate of components weights for the system resulted in specific weight values ranging between 28 W/kg and 41 W/kg. Significant increases in specific power appear possible through development of light weight optical components and advanced recuperator and radiator concepts.

3. Brayton cycle efficiencies of approximately 50, 41, and 28 percent were calculated for a carbon seeded argon working fluid heated to temperatures of 4000 K, 3000 K, and 2000 K, respectively, and a heat rejection temperature of 700 K. For a 320 K heat rejection temperature, Brayton cycle efficiencies of approximately 65, 60, and 51 percent, respectively, were calculated.

4. For a 100 kWe space power system, a state-of-the-art system weight of approximately 3510 kg has been estimated, for a specific power of 28 W/kg. With certain improvements in state-of-the-art technology a system weight of approximately 2420 kg is projected which implies a specific power of 41 W/kg. Achievement of higher specific power values requires development of lightweight collector/concentrators having concentration ratios in the range between 3000 and 10,000.

5. Gas borne carbon particles were determined to be more efficient solar absorbers than high temperature cesium vapor. Results of spectral radiant heat transfer calculations yielded absorption of 86 percent of the incident solar energy by carbon. Corresponding results for cesium vapor absorption ranged between 34 and 64 percent. The lower absorption by cesium is due to its lack of opacity in the infrared portion of the solar spectrum. Relatively uniform volumetric energy absorption was calculated for a carbon seeded stream composed of 0.2 μm dia particles at a density of 3.65 $\mu g/cm^3$, and for cesium vapor pressure between 0.1 to 0.5 atm. The path length through the absorber is approximately 12 cm.

6. Development of the technology for system components of an advanced solar plasma/absorber power system requires additional research in particle laden flow fluid dynamics, radiant heat transfer, high temperature heat exchangers, and lightweight optical concentrators.

INTRODUCTION

Solar energy sustained plasmas may offer the potential for development of high efficiency solar-electric conversion systems. Recent studies reported in Refs. 1 and 2 indicate overall conversion efficiencies of approximately 50 percent or higher might be achieved with development of a reliable energy absorber configuration and advanced high temperature energy extraction technology. Solar energy sustained plasmas appear to be attractive for applications in space including satellite power systems and propulsion or for terrestrial power systems.

Solar energy sustained plasmas are produced by deposition of concentrated solar energy directly into a flowing working fluid to produce temperatures within the working fluid as high as 4000 K. Fluid mechanical confinement of the high temperature plasma is required to isolate the plasma region from surrounding materials which are maintained at lower temperature. Theoretically, this should allow plasma temperatures approaching the sun surface temperature of approximately 5800 K (see Ref. 3) to be produced. Energy transfer from the solar sustained plasma is achieved using advanced concepts such as wave energy exchangers in Brayton or Rankine cycles, MHD (Ref. 2), or photochemical processes.

The objective of this study, described herein, was to develop an initial design for a solar heated plasma/absorber power system. Absorber operating characteristics were analyzed and a reference absorber geometry was selected for incorporation into a Brayton cycle energy extraction system suitable for space power application. An output power level of approximately 100 kWe was selected for the reference power system. Major system components were identified and initial weight estimates made. Also, assessment was made of needed research and technology required to demonstrate technical feasibility of the system concept.

DESCRIPTION OF ABSORBER CONFIGURATIONS

The absorption chamber for the solar heated working fluid is shown in Fig. 1. The cylindrical chamber contains transmission windows through which concentrated solar energy is admitted. The solar energy is collected and concentrated by the large (relative to the absorption chamber) paraboloidal mirrored structure, the back surface of which is shown in the background of Fig. 1. The focused solar image is reflected at the focal plane of the paraboloid by a spherical mirror (not shown) and directed through the open central section of the paraboloidal mirror. The beam is then incident on a mirrored beam splitter (shown in Fig. 1) and subsequently refocused onto the flowing absorber stream inside the receiver absorption chamber. Inlet injectors and exhaust ducts are used to supply and remove the continuously flowing gaseous streams used in the absorber. The opaque inner surface of the chamber is highly reflective to reduce reradiation losses from the absorber stream. Two absorber types were considered: (1) solid particles suspended in a carrier gas and (2) alkali metal vapors in a carrier gas.

Solid Particle Absorber

The solid particle absorber is composed of 0.2 μm-dia carbon particles suspended in a central flowing argon gas stream. This particle size was selected based on Mie absorption coefficient data for carbon which indicates absorption will occur throughout the wavelength range of the solar spectrum. The gas and particles are injected and exhausted at opposite ends of the chamber. The central seeded stream is isolated from the cylindrical wall of the absorption chamber by an annular argon buffer gas stream which flows axially between the absorber region and the chamber peripheral wall. The buffer gas is injected through a series of injectors located in the inlet endwall. The buffer gas exits through an annular exhaust port adjacent to the peripheral wall. Successful fluid dynamic confinement of a particle laden absorber stream has been demonstrated previously in experiments described in Ref. 4.

Metal Vapor Absorber

The metal vapor absorber is composed of cesium vapor in an argon carrier gas. In this configuration, the cesium absorber stream is confined away from the exterior walls of the absorption chamber by a coflowing buffer gas. Results of successful experiments using the coaxial confinement technique **are** reported in Ref. 5. The metal vapor and carrier gas mixture is injected through ports at the center of one chamber endwall. A portion of the flow is removed from the cavity through annular slots in the endwall near the cylindrical wall. The remainder is removed with the absorber stream through a port at the center of the endwall (see Fig. 1).

The buffer gas is expected to remain cool and relatively free of absorber species. However, if radial diffusion of absorber seed material occurs then buffer gas contamination will result. Thus separate clean-up of low contamination levels may be required in the buffer gas circuit. Separation is necessary to prevent increasing energy absorption in the buffer gas and degradation of optical and reflective chamber surfaces, due to coating and/or chemical changes. A particle separator for this purpose is shown in Fig. 1.

Primary Collector and Optics

The size of the illuminated region in the absorption chamber depends upon the optics between the collector and the flowing absorber stream. For the initial design study, specific details of the optical components have not been addressed. To attain a high absorber temperature, it will be necessary to have an optical collection system which has a flux concentration ratio in the approximate range of 3000 to 17,000. For the present studies an ideal paraboloidal collector was assumed to establish the approximate dimension of the collector and absorber. In calculations of radiant energy deposition in the source a 50 percent overall optical efficiency between the collector and the absorber was used.

A circular solar image is produced at the focal plane by the incident rays from all sections of the paraboloidal surface when the collector is aimed directly at the solar source. The solar image is composed of a circular central section (hot spot) which has a uniform high intensity, and an outer annular section which has a decreasing intensity with increasing radius. The diameter of the hot spot is given by

$$D_{HOT} = \alpha f$$

where α is the angular diameter of the sun equal to approximately 0.00931 radians, and f is the collector focal length. The geometry of the collector is shown in Fig. 2; D is the aperture of the collector, and θ_o is the rim angle defined by the included angle between vectors originating at the center of the focal plane and extending to the collector vertex and collector rim, respectively. The equation relating the collector aperture, rim angle, and focal length is given by

$$f = \frac{D}{4}\left[\cot\theta_o + \sqrt{\cot^2\theta_o + 1}\right]$$

The concentration ratio, C, produced at the hot spot is defined as the ratio of the theoretical solar intensity of the hot spot to the solar flux intensity on the collector. The ratio is approximately given by (Ref. 6)

$$C = \frac{4\sin^2\theta_o}{\alpha^2}$$

and is based on the assumption that the solar disc has a uniform intensity, the focal plane images formed by reflection from all points on the paraboloid are ellipses, and the intensity of a given elliptical image is uniform over its surface.

An actual paraboloidal collector concentrator system may have a hot spot diameter approximately equal to that of the perfect paraboloid, but the actual concentration ratio will be reduced. The collector optical efficiency, η_{opt}, is a measure of the transmission through the optical train. A transmission factor is defined which includes surface reflectivity effects, geometrical imperfections, window losses, misalignment, and shadowing of the collector. Collector optical efficiency values in the range of 0.3 to 0.6 (Ref. 6) have been reported for large collectors.

Theoretical collector performance parameters for a single element collector concentrator are presented in Figs. 3 through 5. Figure 3 shows the variation in total power delivered to the high intensity portion of the solar disc for collector apertures of 10 m, 20 m, and 30 m. Results are shown for optical efficiencies of 0.5 and 1.0. The fraction of the total collected energy which passes into the hot spot region varies with collector rim angle and optical efficiency. Specifically,

$$\frac{Q_{HOT}}{Q_{COLL}} = \frac{4 \sin^2 \theta_o}{\alpha^2} \left(\frac{D_{HOT}}{D}\right)^2 \eta_{OPT}$$

The variation of hot spot fractional power with rim angle is shown in Fig. 4 for a collector optical efficiency of 1.0. The remainder of the collected energy passes into a reduced intensity halo region surrounding the hot spot. The results in Fig. 3 indicate an approximately 30-m-dia aperture collector with a 60^o rim angle and a 0.5 optical efficiency could deliver the desired 268.1 kW to the hot spot region of the focal plane.

The variation of focal hot spot intensity with collector rim angle is shown in Fig. 4. Results are presented for overall optical efficiencies of 1.0, 0.8, 0.5, 0.3, and 0.1. A focal hot spot intensity of 2.335 kW/cm^2 is estimated for a collector rim angle of 60^o and optical efficiency of 0.5. The results in Fig. 4 are useful in gauging the combined effects of component imperfection and other optical losses on the maximum hot spot intensity. The hot spot region is where the greatest absorption of energy by the absorber stream will occur.

A reference collector configuration was selected for a solar absorber system designed to operate at an electrical power output of approximately 100 kW. The reference configuration would use a collector mirror equivalent to an ideal paraboloid with a 30 m aperture and a rim angle of 60^o. An optical efficiency

of 0.5 is assumed for the optical system. As indicated in Fig. 5, the total collected power is 954 kW and the diameter of the hot spot is 12.09 cm. The hot spot total intensity is 2.335 kW/cm^2 and the total power incident on the absorber region is 268.1 kW.

ABSORBER HEAT TRANSFER AND FLUID MECHANICS CHARACTERISTICS

Solid Particle Absorber

The solid particle absorber employs 0.2-μm-dia carbon particles suspended in a central flowing argon carrier gas stream. The carbon seeded argon stream is isolated from the cylindrical wall of the absorption chamber by an annular argon buffer gas stream which flows axially between the absorber region and the chamber peripheral wall. The absorber region diameter and length are approximately 12 cm which corresponds to the high intensity focal volume of the reference concentrator.

The theoretical variation in absorption cross section with wavelength is shown in Fig. 6 for 0.2-μm-dia carbon particles. These data were obtained from Ref. 7 and are based on Mie theory calculations for spherical particles. The extraterrestrial fractional solar flux variation with wavelength also is included in Fig. 6. Carbon particles were chosen for the absorbing material because of their large absorption cross section per unit mass, their high melting point, and their low vapor pressure at elevated temperature.

The volumetric energy deposition rate was calculated as a function of radial position within the absorber region for two chamber configurations. Results are presented in Fig. 7 for a chamber with an aluminum reflecting wall. Also shown in Fig. 7 are the results of an aluminum walled chamber for which allowance for window transmission was included. A reflective surface to total surface area ratio of 0.83 was assumed for these later calculations.

The energy deposition corresponding to a carbon density of 3.65 $\mu g/cm^3$ varies from a value of approximately 170 W/cm^3 at the absorber centerline to approximately 205 W/cm^3 at the absorber outer radius for a chamber with no transmission window. With the transmission window included, energy deposition varied from 157 to 183 W/cm^3 between the chamber centerline and the absorber outer radius. The calculation assumed uniform intensity incident upon the outer periphery of the cylindrical absorber stream. The opaque walls of the chamber were assumed to have a reflectivity equal to that of aluminum. The spectral variation of reflectivity for aluminum at a 60^o incident angle was used in these analyses. The reflective properties of aluminum are shown in Fig. 8. The average reflectivity is approximately 0.92 averaged over the solar spectrum. Calculated results showing the fractional distribution of incident and absorbed energy integrated with respect to wavelength are shown in Fig. 9. Approximately 97 percent and 86 percent of the incident energy is absorbed by the carbon for the 100 percent and 83 percent area reflecting chamber wall configurations, respectively. A total incident power of 268.1 kW was used in each case. Two important features of these results are that a small carbon seed density 3.65 $\mu g/cm^3$ results in a significant fraction of incident energy absorbed and that the solid particle carbon absorption is high

for the entire incident solar spectrum. The average carbon density in the absorbing region is only about 1.5 percent of the local argon density in the absorbing region.

Fluid mechanics calculations using the ADD computer program (Ref. 8) were performed to estimate the temperature, velocity, and weight flow profiles within the absorption chamber. The ADD program solves the two-dimensional axisymmetric confined viscous flow equations. An energy source term was included to spatially model the effect of radiant energy deposition within the absorber stream. The energy source distribution used corresponded to that in Fig.10 for the configuration with aluminum reflective walls. The results of the calculations are shown in Figs. 10 and 11 for the inlet location and the exit location at the end of the 12.09 cm heating length. The effect of reradiation was not included in these calculations. The carrier gas is argon and the total chamber pressure is 10 atm. The calculated temperature distribution is shown in Fig. 10. The local temperature varies from approximately 3440 K on the centerline to approximately 4150 K at a radial location of 5.2 cm, then decreases to approximately 300 K at the reflecting peripheral wall. An adiabatic wall boundary condition at the peripheral wall was used in the fluid mechanics calculations.

The total absorbed power is 259.7 kW. Approximately 8.4 kW of incident power is absorbed by the aluminum reflective walls surrounding the absorption chamber. Integrated radial distributions of argon weight flow are shown in Fig. 11a for the entrance and exit locations in the cylindrical heating volume. The total flow rate is 588 g/s of which 0.4 g/s is carbon particles. Essentially all of the enthalpy resides in the argon gas flow. At the inlet station, the total flow rate within the absorber region is approximately 263 g/s and at the exit of the heating volume the total absorber region flow rate is 97 g/s. Approximately 166 g/s diffuses radially out of the absorber region into the buffer region as the flow traverses the heating volume. Approximately 180 kW are associated with the exit station flow from the absorber region, and 79 kW are associated with the buffer region flow. The mass-flow weighted average temperature calculated for the absorber region flow at the exit station is approximately 3800 K and the average temperature of the buffer region flow at the exit station is approximately 611 K for an inlet temperature of 300 K. Diffusion of flow from the absorber region to the buffer region is enhanced by expansion of the absorbing gas as it is being heated. In addition to radial mass transfer, heating of the central absorber region results in axial acceleration of flow. Calculated radial distributions of axial velocity are shown in Fig. 11b. The flow is injected at a velocity of approximately 1.45 m/s on the centerline and accelerates to 6.2 m/s on the centerline at the exit station. The peak velocity of 6.8 m/s occurs near the outside edge of the absorber region and corresponds to the location of the peak temperature.

Metal Vapor Absorber

The alkali metal vapor plasma/absorber configuration employs cesium vapor in a central flowing argon carrier gas stream. In this configuration cesium vapor is confined away from the exterior walls of the absorption chamber. This can be accomplished in a coaxial flow pattern with a cesium and argon mixture absorber region surrounded by argon buffer gas.

Analytical values for the composition of a cesium plasma were obtained over the range of temperatures from 1000 K to 4000 K for the range of total pressures from 0.1 to 1.0 atm. Species number densities are presented in Fig. 12 for the cesium dimer (Cs_2), monomer (Cs), singly charged ion (CS^+), and electrons. Calculations were also made to estimate the relative population of cesium atoms in selected excited states to examine excited-state bound-free transitions which might significantly contribute to plasma absorption at elevated temperatures. The composition data in Fig. 12 indicate the relative contribution of Cs_2 to total plasma opacity will likely decrease as the temperature increases due to the decrease in Cs_2 concentration. Calculated relative population data for the first four low-lying excited states of the Cs atom as a function of temperature are shown in Fig. 13. The results show that at temperatures below 4000 K only the $6p^2p^o$ and $5d^2D$ excited states in cesium can be expected to contribute to the absorption coefficient. Populations for the P and D terms which are doublets were calculated using center-of-gravity or weighted average energies.

The composition results were used to estimate the spectral absorption coefficient for a cesium plasma at a temperature of 3000 K. This data corresponds to that being used in the radiant heat transfer analyses described below. Cross section data for Cs_2 were obtained from Refs. 9, 10, and 11, covering a wavelength range from approximately 0.47 μm to 1.26 μm. The bound-free cross sections covering the wavelength range from 0.2 μm to approximately 0.47 μm of the $6p^2p^o$ and $5d^2D$ states of the Cs atom were obtained from Ref. 12. The absorption coefficients derived from the cross section and composition data for cesium at a temperature of 3000 K and at total pressures of 0.1, 0.5, and 1.0 atm are shown in Fig. 14.

Estimates of the free-free cross section of the Cs^+ ion were made at a temperature of 3000 K using a hydrogenic approximation. At a wavelength of 0.5 μm the free-free absorption coefficient was calculated to be about 4×10^{-5} cm^{-1} and about 7×10^{-4} cm^{-1} at 1.3 μm. Thus, free-free transitions are not expected to significantly contribute to opacity in the temperature range of current interest.

Radiant energy transport calculation for cesium vapor seeded absorber streams were performed for configurations with aluminum reflective chamber walls. Assumed design parameters for the configuration are a total incident solar flux intensity of 2.335 kW/cm^2, total power incident on the absorber of 268.1 kW, and a solar

image diameter of 12.09 cm. Values of the design parameters were selected based on the results of initial scoping studies, and are identical to those used in analyzing the solid particle absorber configuration.

Calculated values for the spectral absorption coefficient of cesium vapor at total pressures of 0.1 atm, 0.5 atm, and 1.0 atm are shown in Fig. 14. The values shown include effects of the cesium decomposition species distribution based on equilibrium calculations at a temperature of 3000 K. Calculated results for the volumetric energy deposition rate resulting from an incident solar flux of 2.335 kW/cm^2 are shown in Fig. 15 for cesium vapor pressures of 0.1, 0.5, and 1.0 atm. The radial distribution of absorbed solar energy is approximately uniform at a cesium pressure of 0.1 atm. The ratio of the volumetric energy deposition at the outside edge of the absorber to that at the centerline of the absorber is approximately two for a cesium pressure of 0.5 atm and five for a cesium pressure of 1.0 atm. Based on these calculations, it was concluded that operation within the range of cesium pressure between 0.1 and 0.5 atm will provide for relatively uniform energy absorption within the plasma absorber region.

The fractional distributions of incident and absorbed energy integrated with respect to wavelength are shown in Fig. 16. Approximately 44, 72, and 78 percent, respectively, of the incident energy is absorbed corresponding to cesium pressures of 0.1, 0.5, and 1.0 atm. The corresponding energy absorbed for the 0.1, 0.5, and 1.0 atm cesium cases are 118.4, 192.2, and 209.2 kW, respectively, for the incident power of 268.1 kW. The spectral results were obtained by segmenting the wavelength range between 0.2 and 1.25 μm into thirteen wavelength groups to approximate the cesium absorption coefficient spectral structure shown in Fig. 14. One additional wavelength group which included the 1.25 to 5.0 μm spectral region, was used to model the nonabsorbing spectral region of cesium vapor. Based on the calculated energy absorption results, the condition corresponding to a cesium pressure of 0.5 atm was selected for the cesium vapor absorber analysis. Calculated volumetric energy deposition for this case varied between approximately 90 W/cm^3 at the absorber centerline to 180 W/cm^3 at the absorber outer boundary. The total absorbed power is 192.2 kW which represents 72 percent of the available incident energy. The remaining 28 percent of the incident energy is absorbed in the aluminum reflective walls surrounding the plasma chamber.

Comparison of results of the cesium absorber calculations with those of the carbon absorber indicate a higher absorption efficiency in favor of the carbon absorber. For the same absorbing physical size and input power the carbon absorber captured 97 percent of the incident energy, whereas the cesium absorber captured only 72 percent of the available incident energy. The differences in absorption efficiency between the carbon and cesium configurations result from the lack of opacity in the infrared portion of the spectrum of cesium.

Fluid mechanics calculations were performed to estimate the temperature, velocity, and weight flow distributions within the flowing absorber stream. The absorber stream is contained within an outer annular argon buffer gas at a total pressure of 10 atm. The absorber stream is fluid dynamically confined away from the optical and reflective surfaces of the plasma chamber.

The calculated temperature distribution at the exit plane of the cylindrical heating volume is shown in Fig. 17. The heating length was assumed equal to the 12.09 cm solar image diameter. Absorber stream inlet conditions are temperature and velocity of 900 K and 2.8 m/s, respectively. The calculated temperature at the exit plane varies from 2400 K on the centerline to approximately 4800 K near the outer periphery of the absorber region. The temperature then decreases to 900 K at the reflecting peripheral wall. The calculations do not include reradiation from the absorber region which would reduce slightly the temperature level of the central absorber stream (see following subsection).

Integrated radial distributions of cesium and argon weight flow are shown in Fig. 18a for the heating volume entrance and exit planes. The total weight flow rate of 403 g/s includes 27 g/s of cesium vapor. Approximately 90 percent of the energy absorbed appears as enthalpy in the argon gas flow. The total flow rate within the absorber region varies from 187 g/s at the inlet plane to 107 g/s at the exit plane. The difference between these flow rates is equal to the mass transport from the central absorber stream to the buffer region by radial diffusion as the flow passes through the heating volume. Approximately 125.8 kW are associated with the exit plane flow from the absorber region, and 66.4 kW are associated with the buffer region flow. Calculated average temperatures for the absorber and buffer region flows at the exit plane are 3510 K and 1340 K, respectively. The heating of the central absorber region results in an axial acceleration of the flow. Calculated radial distributions of axial velocity are shown in Fig. 18b. The flow which was assumed to be injected at a velocity of approximately 2.8 m/s on the centerline, accelerates to 5.7 m/s on the centerline at the exit plane. The peak axial velocity of 6.9 m/s occurs at the location of maximum temperature near the periphery of the absorber stream.

Estimates of Absorber Reradiation

An increasing amount of the absorbed solar energy will be reradiated from the absorber as the temperature is increased. This effect will ultimately limit the temperature to which the flowing absorber stream can be heated. A series of spectral radiation transport calculations were performed to estimate the maximum effective radiating temperature for both carbon particle seeded absorber streams and cesium vapor absorber streams. The wavelength range was subdivided into 10 and 14 wavelength groups, respectively, for the carbon and cesium transport calculation.

A one-dimensional cylindrical model of the absorber stream was used in the analysis, with provision for including a nonperfect spectral reflecting boundary at the absorption chamber peripheral wall. Spatial and spectrally varying absorption and emission coefficients were used in the numerical solution of the radiation transport equation (Refs. 13 and 14) within the absorber stream. Flow effects are neglected in the model which allows calculation of the maximum effective radiating temperature at the exit end of the heating volume. The assumption is made that continued solar illumination results in no further increase in enthalpy of the gas stream. This implies that the incident illumination is being exactly balanced by absorption or losses at the peripheral wall due to the transmitted solar flux and to the reradiated flux. Multiple reflections at the wall were considered. Additional assumptions made were: a constant temperature gas, uniform solar flux at the focal plane of the absorbing region, and the flux distributed over the cylindrical absorber surface is such that the total power incident on the absorber volume is conserved. The calculated variation in the net reradiated flux at the outer cylindrical surface of the absorber with effective radiating temperature is shown in Fig. 19 for focal plane incident fluxes of 0.4048, 1.367, and 2.335 kW/cm^2. The fluxes correspond approximately to solar concentration ratios of 3000, 10,000, and 17,300, respectively. Radiating temperatures vary between 2275 K and 3275 K for a carbon absorber with a density of 3.65 $\mu g/cm^3$ and no reflecting surface at the peripheral wall.

A second series of calculations applicable to the carbon absorber included an aluminum reflecting peripheral wall and an allowance for a transmission window. The ratio of reflecting surface area to total peripheral surface area was 0.83, which corresponds to a window area equal to 0.17 times the total surface area. The effect of the reflecting surface is to trap some of the transmitted and reradiated energy. The calculated results, shown in Fig. 19, indicate increased absorber effective radiating temperatures between 3300 K and 4275 K for incident fluxes between 0.4048 and 2.335 kW/cm^2. Similar results are also shown in Fig. 19 for cesium vapor absorber streams for which the cesium vapor pressure is 0.1 and 0.5 atm. The cesium calculations also assumed an aluminum reflecting wall with a 0.83 reflecting surface area ratio. The results in Fig. 19 indicate a cesium vapor absorber at 0.1 atm pressure is not as efficient an absorber as one at 0.5 atm pressure in that the 0.1 atm cesium absorber requires a higher temperature to radiate a given amount of energy. Further, the carbon seeded absorber at a seed density of 3.65 $\mu g/cm^3$ is more efficient than either of the cesium absorber configurations. The carbon absorber is capable of reradiating its solar absorbed energy at a lower temperature for the peripheral wall configuration. For comparison, the upper curve in Fig. 19 corresponds to that of a black-body radiator and is a limiting case.

The fraction of absorbed energy for the different absorber configurations can be obtained by comparing the corresponding radiated fluxes with the blackbody radiator. Approximately 34, 64, and 86 percent of the incident solar energy is absorbed by the 0.1 atm cesium, 0.5 atm cesium, and 3.65 $\mu g/cm^2$ carbon absorbers, respectively.

The effect of vaporization of carbon particles at elevated temperature was not included in these results. The effect of vaporization would be to reduce the temperatures shown in Fig. 19. At 3000 K, the vapor pressure of carbon is approximately 2.6×10^{-4} atm. Below 3000 K the energy associated with vaporization is probably small; however, above 3000 K it would be expected to become a more important factor and should be considered in more detailed studies. Also, the cesium absorption cross section data used in the calculations was evaluated at a temperature of 3000 K. Cesium absorption is expected to decrease based on the decreasing absorbing species density at high temperatures as indicated in Fig. 12. These effects coupled with the convective removal of energy in a flowing absorber would further reduce maximum temperatures below those predicted in Fig. 19, based solely on reradiation considerations.

POWER CONVERSION SYSTEM STUDIES

Absorber characteristics were determined for both carbon particle (0.2-μm-dia) absorber and cesium vapor absorber configurations. Working fluid temperatures are estimated to be in the range of 2000 to 4000 K. Two possible energy extraction systems which accomplish efficient conversion of energy in this temperature range are MHD and modified gas turbine cycles. MHD conversion is usually limited to working fluid temperatures greater than approximately 2300 K (Ref. 15) because of the rapid decrease in electrical conductivity at temperatures below this level. In conventional cesium and/or potassium seeded fossil fueled combustion MHD systems, a bottoming cycle is generally used to extract energy at working fluid temperatures below about 2300 K.

Cycle Performance Analyses

In the current study, emphasis was placed on use of a modified Brayton cycle for high temperature energy conversion. Due to material limitations on turbine inlet temperature in Brayton cycle gas turbine energy extraction systems, the high working fluid temperatures ($\approx$ 3000 K) characteristic of the solar plasma systems cannot be used directly. A possible solution to circumvent the turbine inlet temperature constraint of current gas turbines was proposed in Ref. 16 and expanded upon in Refs. 17, 18, and 19. The method uses a direct gas-to-gas energy exchanger in which the expansion energy of a high temperature fluid is transferred directly to a cooler fluid. Conceptually, the energy exchanger is a series of ducts which are sequentially filled with cold fluid at low pressure. The high temperature fluid is sequentially brought into direct thermal contact with the cooler fluid. The action by the hot fluid is to compress, heat, and expel the cold fluid from the tubes in a quasi-steady fashion. The energy exchanger operates on nonsteady flow principles and compression of the cold fluid results from aerodynamic shock processes. Since the tube walls are alternatively exposed to hot and cold fluid, the temperature of the wall may be considerably less than the maximum fluid temperature. Development of an efficient energy exchanger may permit a high efficiency thermal cycle to be attained through coupling the high temperature solar plasma source to advanced high temperature turbines. Small-scale experiments to demonstrate energy exchanger performance are being pursued (Ref. 19) under DOE sponsorship.

In a solar plasma energy extraction cycle, the energy exchanger could be located between the plasma source and the turbine. A regenerator would also be used in the cycle. The cycle configuration is shown in Fig. 20. Two separate flow circuits are utilized. The absorber stream composed of gas borne carbon particles in argon serves as the hot high pressure fluid in the energy exchanger.

Expansion of this fluid in the energy exchanger results in transfer of enthalpy from the fluid. Upon exiting the energy exchanger the fluid enters the regenerator. The fluid is subsequently recompressed and preheated prior to reinjection into the absorption chamber. The second flow circuit consists of a working fluid composed of a mixture of argon and helium. The working fluid is compressed and heated within the energy exchanger as a result of its interaction with the hot working fluid, and subsequently expanded in a power turbine. According to Ref. 18, the efficiency of the energy exchanger is highest if the speed of sound in both the hot and cold fluids are matched. The speed of sound in gases is proportional to the square root of the product of the ratio of specific heats and temperature, divided by molecular weight. Through selection of the desired operating temperature range in the energy exchanger, the composition of the cold fluid may be tailored to produce the highest energy exchanger efficiency.

A thermodynamic cycle selected for possible space application is shown in Fig. 20. Cycle parameters selected for the argon/carbon seeded working fluid configuration are a peak temperature of 3000 K, turbine inlet temperature of 1200 K, and waste-heat radiating temperature of 700 K. Intercooling is employed between the three compression stages. The maximum pressure is 10 atm in both hot and cold working fluid circuits. Turbine and compressor efficiencies of 0.9 and regenerator effectiveness of 0.9 were assumed for the cycle. The cycle efficiency calculated is 42 percent for an energy exchanger component efficiency of 85 percent. The cycle efficiency is a maximum at a compressor pressure ratio of 4.0. This is shown in Fig. 21 where the variation of cycle efficiency with pressure ratio is shown for energy exchanger component efficiencies of 90 percent, 85 percent, and 70 percent, and hot fluid energy exchanger inlet temperatures of 2000 K, 3000 K, and 4000 K. Cycle efficiency of 28 and 50 percent was calculated for energy exchanger inlet temperatures of 2000 K and 4000 K, respectively, at an energy exchanger efficiency of 85 percent. Cycle efficiencies of 31 and 52 percent were calculated for energy exchanger inlet temperatures of 2000 and 4000 K, respectively, at an energy exchanger efficiency of 90 percent. For an energy exchanger efficiency of 70 percent, the corresponding cycle efficiencies were reduced by approximately 9 percent, when compared to cycles with energy exchanger efficiency of 85 percent.

The calculated efficiencies for the solar plasma energy exchanger/gas turbine cycles are significantly greater than the 15 to 18 percent efficiencies which are characteristic of state-of-the-art space power systems currently under development by DOE and NASA (see Refs. 20 and 21).

In the modified Brayton cycle represented in Fig. 20, the most severe material temperature constraint is probably in the regenerator. The variation in regenerator inlet temperature with pressure ratio for the carbon particle absorber working fluid is shown in Fig. 22. Results are shown for energy exchanger inlet temperatures of 2000 K, 3000 K, and 4000 K, and the energy exchanger

efficiencies of 0.70, 0.85, and 0.90. A solar heated working fluid at 4000 K appears to be beyond the state-of-the-art for regenerators in cycles with maximum efficiency. However, in a less efficient cycle ($\approx$44 percent), a regenrator inlet temperature of 1900 K results for an expansion ratio of approximately 11 and maximum working fluid temperature of 4000 K. In a joint U.S.-USSR experimental program to develop MHD electrical power generation (Ref. 15), high-temperature regenerators with pebble matrices are being developed to heat air and other gases to temperatures 1775-2275 K. Ceramic spheres of high-purity alumina and calcia-stabilized zirconia have been used for preheating air to 1775-2325 K for an extended period in a heating-cooling cycle operation. Development of currently conceived exotic high temperature regenerative heat exchangers for small power extraction systems would be required to permit use of solar heated working fluids to a temperature of approximately 3000 K or higher.

Limited systems studies were also conducted for a heat rejection temperature of 320 K which is typical for possible terrestrial applications. The results are shown in Fig. 23. Cycle efficiencies between approximately 40 to 65 percent were calculated for carbon seeded argon working fluid temperatures between 2000 K and 4000 K and pressure ratios between 2.0 and 4.75.

Estimates of cycle efficiency were also made for a cesium vapor-argon working fluid at a heat rejection temperature of 900 K. Modified Brayton cycle efficiencies between 8 and 40 percent were calculated for working fluid temperatures between 2000 and 4000 K. The results are shown in Fig. 24. For the cesium absorber, the effect of energy exchanger efficiency on the cycle efficiency is more significant than for the carbon absorber conditions. The results indicate the importance of high energy exchanger efficiency in cycles with a high rejection temperature.

Component Weight Estimates

Estimates of the masses of the major components of the reference carbon absorber system configuration are shown in TABLE I. The three principal advanced state-of-the-art components are the heat rejection radiator, the solar collector structure, and the high temperature regenerator. The heat rejection radiators would be stainless steel or refractory metals. Radiating temperatures between 700 and 940 K were assumed (see Fig. 20). A separate liquid metal coolant circuit would be used for the radiators to reduce the required radiator area. The circuit would couple to the working fluid circuits secondary heat exchangers. For purposes of estimating weight, the solar concentrator was assumed to be composed of a series of front surface reflectors. The deployable concentrator surfaces might be similar to those considered for the thermal engine Solar Power Satellite (SPS) concept (Ref. 22). Individual heliostats are arranged in a paraboloidal configuration to produce concentration ratios in the range of 3000 to 17,000. A mirror mass

of approximately 0.35 kg/m^2 has been used for estimating purposes. The high temperature regenerator would be an advanced state-of-the-art ceramic pebble bed recuperator. This type of regenerator should be capable of operation in the range of 1725 to 2275 K (Ref. 15). The energy exchanger is also an advanced state-of-the-art component. Energy exchanger technology is currently under development (Ref. 19). The mass of the energy exchanger is assumed to be comparable to conventional turbomachinery. The total mass of the major system components is 3510 kg for an approximate 100 kWe Power System. Additional system components included in the total system mass are the absorption chamber, electrical generator, and rotating machinery.

Also included in TABLE I is an estimate of total system mass for a system with advanced state-of-the-art concentrator/collector and electrical generator components. The advanced state-of-the-art solar collector and structure mass is based on a specific collector mass of 0.07 kg/m^2 (Ref. 23). The generator is a superconducting type for which a cryogenic circuit is required. The total mass of the advanced system is 2420 kg for a specific energy corresponding to 41 W/kg. Further reductions in system mass are possible through development of ultra-light optics and novel space radiator concepts such as those in Ref. 24.

TECHNOLOGY REQUIREMENTS

The solar plasma/absorber power system concept has the potential for high efficiency because of its high working fluid temperature capability. Successful implementation of the concept will require technological advancements in the major system components. This section provides a limited review of the technological status of the major system components.

Absorption Chamber

The component central to the concept is the absorption chamber. There appears to be no technology barrier which prevents a flowing absorber from being radiatively heated to high temperatures. It is a matter of producing a high incident flux and reducing reradiation losses. A tungsten seeded argon stream has been radiatively heated in a small test configuration to a temperature of approximately 4500 K for a limited short (1/2 s) run time (Ref. 25), and to lower temperatures for longer (10-30 s) run time. Continuous or long running test times were not within the scope of the previous research program. Crucial to the absorber is the ability to inject submicron size solid particles such as carbon with a carrier gas into the absorption chamber and maintain a relatively uniformly seeded stream in a regulated and controlled manner. Satisfactory results have been obtained in short run-time tests with regard to maintaining clean chamber walls, however, similar buffer confinement must be demonstrated in a continuous long run time test program. The appearance of high seed density streamers was observed in previous research. The source of these streamers was not fully understood. Additional engineering investigations will be required to generate a uniformly seeded stream, which will be conducive to approximately uniform heating of the absorber stream. This would involve further development of particle feeder systems, but no significant impediment to the flowing absorber concept is obvious at this time.

Development of the exhaust endwall geometry is required such that the hot and cold flowing streams can be collected and channeled to the energy extraction system (hot flow) or recirculated through the absorption chamber (cold flow). The hot flow duct will present the major problem at high temperature. Transpiration or internally cooled ducts are possible design alternatives for this component. This likewise is considered to be a feasible engineering development effort.

Regenerator

The regenerator in the power extraction cycle is a high technology component in the power system. Inlet regenerator temperatures in the range of 1900 to 2300 K are necessary for the higher efficiency ($\approx 50\%$) cycles. Refractor-type regenerative heat exchangers are considered capable of operation at high temperature and are being developed in the U.S. and USSR MHD electrical power generation programs (Refs. 26 and 27). These regenerators operate on the principle in which heat is transferred through a medium that is cyclically heated by a hot fluid and subsequently cooled by a cool fluid. A fixed-bed regenerator operates intermittently due to its cycling nature, so that the regenerator subsystem may require several units configured in a parallel with cooled switch-over valves. This allows a continuous flow of gas which has a temperature varying between a maximum and minimum value in both the heating and cooling parts of the cycle. Alumina (Al_2O_3), magnesia (M_gO), zirconia (ZrO_2), and their composites are normally considered for use in the high temperature regimes. A pebble bed matrix has good heat transfer characteristics and can be made compact for minimum weight due to a low thermal inertia and an accompanying small cycle period. However, they are limited by pressure drop and thermal stress considerations. Typically pebble sizes are in the range of 2 to 5 cm and are inexpensive to manufacture. Dense ceramic spheres of high purity alumina and calcia-stabilized zirconia were tested (Ref. 15) extensively (15000 h) in a pebble-bed heater, preheating air to 1775-2325 K. Alumina was used up to temperature 1975 K and the zirconia up to the high temperature with no significant structural problems. The regenerator component is an advanced state-of-the-art technology for which considerable development is being performed, notably in the MHD program. However, further development will be required to develop high temperature regenerators with low weight for space power systems.

Energy Exchanger

The energy exchanger is used for transfer of work by unsteady gas dynamic processes. Expansion and cooling of the hot fluid and compression and heating of a cool fluid occurs within a series of tubes in a rotating drum. Fixed injection and exhaust manifolds are used. Individual tubes are exposed to high temperature fluid for a short time so that wall temperatures are well below the peak gas temperature. The principle was first demonstrated by C. Seippel (Ref. 16) in a device which transferred 69 percent of the available expansion work with a compression ratio of 2.5. Additional experiments were conducted at Cornell (Ref. 17) in which an energy exchanger was used as a superheater to heat air to 4500 K by helium gas at less than 1000 K. This is a reverse operation to that required in a power extraction cycle, but the concept of the energy exchanger does appear to be reversible. The energy exchanger serves as a coupling device to use a lighter lower temperature working fluid (≈ 1200 K) in an advanced gas

turbine circuit to extract work from the energy which is transferred from the hot primary working fluid stream. The value of the energy exchanger comes from its potential for handling high temperature working fluid (2000 K to 4000 K). The gas turbine gas circuit can then be tailored to temperature levels which are closer to state-of-the-art technology. Optimum performance characteristics for the energy exchanger have not been determined; however, preliminary studies and tests indicate a unique potential for high efficiency cycles may be within the range of engineering development (Refs. 18 and 28).

Alkali Metal Handling Technology

Alkali metal handling and compatibility with system components is a consideration for the absorber configuration with cesium vapor. A review of alkali metal technology is given in Ref. 29 relative to Rankine energy conversion systems for electrical power in space which were being developed under NASA and AEC programs. Corrosion by alkali metals has been reduced to negligible amounts up to temperatures of approximately 1370 K. This has been accomplished by use of refractory metals for containment and structural materials and by minimizing the oxygen content throughout the system. Oxygen getters such as Hf and Zr are alloyed with the refractories. TZM alloy (MO - 0.6 Ti - 0.1 Zr - 0.035 C) has shown promise as having good resistance to alkali metal attack at elevated temperature. A foundation of basic technology has been developed for an alkali metal, Rankine cycle turbogenerator. A potassium loop, 5000 hr endurance test was performed on a three-stage turbine using TZM for inlet temperature of 1100 K, flow rate of 1 kg/s, and vapor quality between 100 and 87 percent for power of 235 kWe. Start-up and subsequent operation was trouble free (Ref. 29).

A current DOE program uses a potassium vapor topping cycle for increasing efficiency of a Rankine vapor cycle with turbine inlet temperature of 1140 K and is being investigated at Oak Ridge National Laboratory (ORNL) (Ref. 30). This cycle is superimposed on a conventional steam cycle with turbine inlet temperature of 810 K, for a combined 50 percent cycle.

Cycles with higher temperatures would require further development on corrosion resistance capability of the refractory alloys, or perhaps the development of ceramic materials used in conjunction with the alkali metals.

Solar Collector/Concentrator

The collector/concentrator for solar powered systems is a key technology. To obtain a high working fluid temperature in a flowing absorber, high solar concentration ratios are required (> 3000). Rigid paraboloidal structures with high concentration characteristics have high specific mass in the range of approximately 2 kg/m^2 (Ref. 22). This type of collector will represent a significant fraction of the total mass in systems of currently developed component technologies. Studies have also been made (Ref. 23) of a nonrigid concentrator for a space system. Individual reflectors cover the surface formed by a light support framework and are positioned by a servomechanism mounted between the mirror and the frame. The reflector facet consists of a light framework which tensions an aluminized Kapton film mirror. A specific mass of 0.07 kg/m^2 has been projected for the faceted collector structure. Further development will be required to develop reliable, low weight reflector tracking and pointing systems, to attain high solar concentration ratios. Prospects for development of light weight collector/concentrator configurations appear promising. In this study, a collector specific mass of 0.35 kg/m^2 was used for the state-of-the-art collector structure and a specific mass of 0.07 kg/m^2 was used for the advanced state-of-the-art collector structure.

PROOF-OF-PRINCIPLE EXPERIMENTS

Development of the absorption chamber is central to the solar plasma concept and might be given initial priority over other system components such as collector/concentration optical trains, high temperature turbines, MHD power extraction duct, high temperature regenerative heat exchangers, energy exchangers, and space radiators which have had significantly greater development efforts in other programs.

The successful implementation of solid particle absorber concept requires that the fluid mechanics and heat transfer characteristics of the flowing absorber can be controlled and regulated in a known manner. Experiments are required to develop injection and geometry requirements of both the absorber and buffer flow streams so that the absorber stream is confined away from the chamber walls and contained within a central region of the flow such that diffusion of the absorber does not occur into the outer buffer stream. As a result of the present study, a carbon particle seeded argon absorber configuration appears to be a more efficient absorber.

Additional cold flow tests are required in a fused-silica walled absorption chamber with inlet and exhaust endwall geometry to simulate the confinement of a seeded stream by an outer buffer stream. Inlet flow conditions such as buffer layer width, injection velocity, seeding techniques, particle size, particle to carrier flow rate must be varied to establish confinement and containment conditions. Scanning optical absorption measurements should be made to estimate the degree of uniformity in the seeded stream, physical dimensions of the seeded stream, and degree of particle coating of peripheral walls. The concept further requires that small (submicron) solid particles be introduced in a controlled fashion. Uniformity of the particles must be controlled to the extent that no significant regions of high seed density occur in the flowing central absorber region. This will allow approximately uniform heating of the absorber stream. A high pressure solid particle feeder concept (Ref. 31) which was developed for providing seeded carrier and buffer gas flow streams might be modified to provide similar flow streams to a simulated solar absorption chamber. Tests should be conducted to determine inlet conditions of fluid dynamics parameters and inlet seed distribution techniques that are required to provide a confined seeded stream. At the exhaust end of the absorption chamber, the central absorber stream will be eventually heated to high temperature. The outer buffer stream will be considerably lower in temperature, increasing in temperature primarily due to radial diffusion of seeded gas out into this region. The energy extraction system of the solar absorber concept will use only the central seeded stream as the heat source so that an exhaust geometry is required to separately handle the hot absorber and cold buffer flows. Exhaust endwall configurations must be developed to separate and collect the exhaust flow into at least two different

plenum ducts. Methods must be developed to determine bulk temperatures for the flow in the individual plenum regions.

Hot flow tests should also be conducted in which the particle seeded stream is radiatively heated. Initially, the absorption chamber walls could be fused-silica so that optical diagnostics can be more easily used to evaluate the effect of test conditions on the confinement, containment, and uniformity of the absorber stream as well as inlet and exit chamber flow patterns. A mirrored configuration could partially surround the flow chamber to reduce possible transmission and reradiation losses, resulting in the attainment of high temperatures in the flowing stream.

The heated flow tests are dependent on a radiant energy source being used. To avoid the need in these exploratory tests to design and construct a solar collector and concentrator optical system which can produce a small area, high intensity flux, and can deliver it to the absorber stream, a dc arc radiant energy source can be used to simulate a concentrated solar source. The spectral content of the dc arc is similar to the solar spectrum between the wavelength range of 0.2 to 1.3 micron. Incident flux level between 0.15 and 1.1 kW/cm^2 can be obtained for radiantly heating the absorber stream. Several possible illumination geometries could be investigated to determine combined absorber and dc arc source configurations which produce uniform heating in the absorber stream, and reduced radiation losses.

A third series of tests should be performed using an absorption chamber which has aluminum reflective peripheral walls on the interior surfaces of the chamber, except for a transmission portal through which the radiant flux will be incident on the absorber stream. This configuration would be similar to the chamber presently conceived for a reference solar sustained plasma system. The geometry and flow conditions for this configuration should be developed based on the prior heated test series. Because of the reflective surfaces, higher absorber temperatures (> 2000 K) are expected due to reduced optical losses, and more uniform volumetric energy absorption should be possible. Diagnostic techniques developed during the initial cold flow and hot flow tests with fused-silica walls may require some modifications for monitoring of test data in these experiments. The results of this series will be used to develop design data for the full scale reference 100 kWe configuration. This absorption chamber could be conceptually verified by conducting solar heated tests at a currently available test site such as the Solar Tehrmal Test Facility (STTF). This facility is operated for Department of Energy (DOE) by Sandia Laboratories to advance the development of solar thermal electric power to a commercial scale (Ref. 3).

REFERENCES

1. Mattick, A. J.: Absorption of Radiation By Alkali Vapors. Presented at Third NASA Conference on Radiation Energy Conversion, Moffett Field, CA., 1978.

2. Palmer, J. A.: Radiatively Sustained Cesium Plasmas for Solar Electric Conversion. Presented at Third NASA Conference on Radiation Energy Conversion, Moffett Field, CA., 1978.

3. Thekaekara, M. P.: Data on Incident Solar Radiation. Supplement to Proc. 20th Annual Meeting of Institute for Environmental Science, Vol. 21, 1974.

4. Bennett, J. C. and B. V. Johnson: Experimental Study of One- and Two-Component Low Turbulence Confined Coaxial Flow. United Technologies Research Center Report J910934-10, 1971.

5. Jaminet, J. F. and A. E. Mensing: Experimental Investigation of Simulated-Fuel Containment in R-F Heated and Unheated Two-Component Vortexes. United Aircraft Research Laboratories Report J-910900-2, prepared under Contract SNPC-70, September 1970.

6. Bliss, R. W.: Notes on Performance Design of Parabolic Solar Furnaces. J. of Solar Energy Science and Engineering, Vol. I, No. 1, January 1957, pp 22-29.

7. Krascella, N. L.: Theoretical Investigation of the Absorption and Scattering Characteristics of Small Particles; prepared under Contract No. NASw-847 by United Aircraft Corporation. NASA Contractor Report NASA CR-210, April 1965.

8. Anderson, O. L.: User's Manual for a Finite Difference Calculation of Turbulent Swirling Compressible Flow in Axisymmetric Duct with Struts and Slot Cooled Walls. Prepared by United Aircraft Research Laboratories for U.S. Army Air Mobility Research and Development Laboratory, Ft. Eustis, Va., Report USAAMRDL-TR-74-50, Under Contract DAAJ02-73-C-0037, 1974.

9. Wechsler, A. E.: Characteristics of Metal Vapor. Arthur D. Little, Inc., Cambridge, MA., Aerospace Research Laboratories Report ARL 66-0004, January 1966.

10. Lapp, M. and L. P. Harris: Absorption Cross Sections of Alkali-Vapor Molecules. Journal of Quantitative Spectroscopy and Radiative Transfer, Vol. 6, 1966, pp 169-179.

REFERENCES (Continued)

11. Benedict, R. P., D. L. Drummond, and L. A. Schlie: Absorption Spectra of the CS Molecule. Journal of Chemical Physics, Vol. 66, No. 10, May 1977, pp 4600-4607.

12. Moskvin, Yu. V.: Photoionization of Atoms and Recombination of Ions in the Vapors of Alkali Metals. Optics and Spectroscopy, Vol. 15, No. 5, 1963, pp 316-318.

13. Engle, W. W., Jr.: A User's Manual for ANISN, A One-Dimensional Discrete Ordinates Transport Code with Anisotropic Scattering. Union Carbide Corp. Report K-1693, 1967.

14. Rodgers, R. J., T. S. Latham, H. E. Bauer: Analytical Studies of Nuclear Light Bulb Engine Radiant Heat Transfer and Performance Characteristics. United Aircraft Research Laboratories Report K-910900-10, prepared under NASA Contract SNPC-70, September 1971.

15. Petrick, M. (USA), B. YA. Shumyatsky (USSR), Editors: Open-Cycle Magnetohydrodynamic Electrical Power Generation. A Joint USA/USSR Publication. Department of Energy Report DOE-TR-119, Argonne National Laboratory, Argonne, Illinois, 1978.

16. Seippel, C.: Pressure Exchanger. U.S. Patent No. 2,399,394, 1946.

17. Kantrowitz, A., A. Hertzberg, E. McDonald, and E. Resler: Heat Engines Based on Wave Processes. Cornell University Graduate School of Aeronautical Engineering Report, 1948.

18. Weatherston, R. C. and A. Hertzberg: The Energy Exchanger, A New Concept for High-Efficiency Gas Turbine Cycles. Transactions of the ASME, Journal of Engineering for Power, April 1967, p. 217.

19. Taussig, R. T., P. H. Rose, J. F. Zumdieck, and A. Hertzberg: Energy Exchanger Technology Applied to Laser Heated Engine. Presented at the Third Conference on Radiation Energy Conversion, NASA Ames Research Center, 26-28 January 1978.

20. Klass, P. J.: Vulnerability Shifts Space Power Focus. Aviation Week and Space Technology, Vol. 110, No. 2, 8 January 1979, pp 58-59.

REFERENCES (Continued)

21. Mullin, J. P. and L. B. Holcomb: Technology for Power in Space. Proceedings of the 12th Intersociety Energy Conversion Engineering Conference, Washington, D.C., Vol. II, 28 August - 2 September 1977, pp 1362-1369.

22. Gregory, D. L.: Thermal Engine Solar Power Satellites. Proceedings of the 12th Intersociety Energy Conversion Engineering Conference, Washington, D.C., 28 August - 2 September 1977, pp 1386-1390.

23. Considine, D. M. (Ed.): Energy Technology Handbook. McGraw-Hill Book Co., New York, 1977.

24. Bekey, I. and W. Blocker: High Efficiency Low Cost Solar Cell Power. Aeronautics and Astronautics, Nov. 1978, pp 32-38.

25. Klein, J. F.: Nuclear Light Bulb Propellant Heating Simulation Using a Tungsten Particle/Argon Aerosol and Radiation from a DC Arc Surrounded by a Segmented Mirror Cavity. United Aircraft Research Laboratories Report L-910900-13, prepared under NASA Contract SNPC-70, September 1972.

26. White, L. R., D. G. DeCoursin, and A. W. Postlethwaite: The Status of Air Heater Development in the United States for MHD System. MHD Fourth U.S.-U.S.S.R. Colloquium on Magnetohydrodynamics Electrical Power Generation, Washington DC, U.S. Department of Energy Report CONF-781009, UC-70g, October 5-6, 1978.

27. Volovik, A. V., et al: High Temperature Air Preheaters for a Commercial Scale MHD Power Plant. MHD Fourth US-USSR Colloquium on Magnetohydrodynamic Electrical Power Generation, Washington DC, US Department of Energy Report CONF-781009, UC-90g, October 5-6, 1978.

28. Taussig, R. T.: Energy Exchanger Development Program. Mathematical Sciences Northwest, Inc., Bellevue, Washington, Nov. 1978.

29. Manson, S. V.: A Review of the Alkali Metal Rankine Technology Program. Journal of Spacecraft and Rockets, Vol. 5, No. 11, November 1968.

30. Holcomb, R. S.: Potassium Vapor Topping Cycle Technical Progress Report for Period July 1, 1977 - September 30, 1977. Oak Ridge National Laboratories Report ORNL/TM-6153, February 1978.

REFERENCES (Concluded)

31. Klein, J. F.: Experiments to Simulate Heating of the Propellant in a Nuclear Light Bulb Engine Using Thermal Radiation from a D-C Arc Radiant Energy Source. United Aircraft Research Laboratories Report K-910900-8, prepared under Contract SNPC-70, September 1971.

32. Darsey, D. M., et al.: Solar Thermal Test Facility Experimental Manual. Prepared by Sandia Laboratories for U. S. Department of Energy, Report SAND77-1173, October 1977.

LIST OF SYMBOLS

C	Solar flux concentration ratio, dimensionless
D	Solar collector aperture, m
D_{HOT}	Concentrated solar image diameter at focal plane of collector, cm
F_A	Spectral fraction of solar flux absorbed, dimensionless
F_I	Spectral fraction of incident solar flux, dimensionless
f	Focal length of collector, m
I_F	Focal plane hot spot intensity, kW/CM^2
Ni	Number density, cm^{-3}
Nm/N_{TOTAL}	Relative population, dimensionless
P	Pressure, atm
PR	Pressure ratio, dimensionless
Q_{ABS}	Total absorbed power, kW
Q_{COLL}	Total collected power, kW
Q_{HOT}	Total hot spot power, kW
Q_v	Volumetric energy deposition, w/cm^3
R	Radius, cm
R_λ	Spectral reflectivity, dimensionless
T	Temperature, deg K
$\bar{T}$	Bulk gas temperature, deg K
T*	Radiating temperature, deg K
T_{BB}*	Effective blackbody radiating temperature, deg K
Tregn	Inlet temperature to regenerator, deg K

LIST OF SYMBOLS (Concluded)

V	Velocity, m/s
W	Flow rate, g/s
α	Angular solar diameter, .00931 radians
$\overline{\alpha}$	Spectral absorption coefficient, cm^{-1}
η_{cyc}	Brayton cycle efficiency, dimensionless
η_{OPT}	Optical train efficiency, dimensionless
Θ	Angle formed by reflected ray from collector mirror and plane perpendicular to focal plane, degree
Θ_o	Collector rim angle, degree
λ	Wavelength, micron
μ/ρ	Spectral mass absorption coefficient, cm^2/g
ρ	Distance from mirror segment to center of solar image at the focal plane, m
ϕ	Angle of incidence, deg

TABLE I

REFERENCE CONFIGURATION MAJOR COMPONENT MASSES

	State-of-the-Art Component Mass kg	Advanced State-of-the-Art Component Mass kg
Radiator @ 700 K	450	450
Collector and Structure	1020	200
Combined Rotating Machinery	230	230
Recuperator	840	840
Generator	540	270
Energy Exchanger	230	230
Absorption Chamber & Feeder	200	200
TOTAL	3510	2420

TABLE II

PROOF-OF-PRINCIPLE EXPERIMENTS FOR SOLID PARTICLE SEEDED ABSORBER

I.	COLD FLOW CONFINEMENT TESTS Design and Construct SiO_2 Chamber Solid Particle Feeder System Exhaust Endwall Two Zone Flow Collector
II.	INITIAL HOT FLOW CONFINEMENT TESTS (SiO_2 Chamber) Solar Simulated DC Arc Source External Mirror Configuration Temperature Range 1000 K to 2000 K
III.	HOT FLOW CONFINEMENT TESTS Reflective Inner Wall Surface Transmission Port Solar Simulated DC Arc Source Temperature > 2000 K Develop Design Data for Solar Source Tests

SOLAR SUSTAINED PLASMA / ABSORBER RECEIVER CONFIGURATION

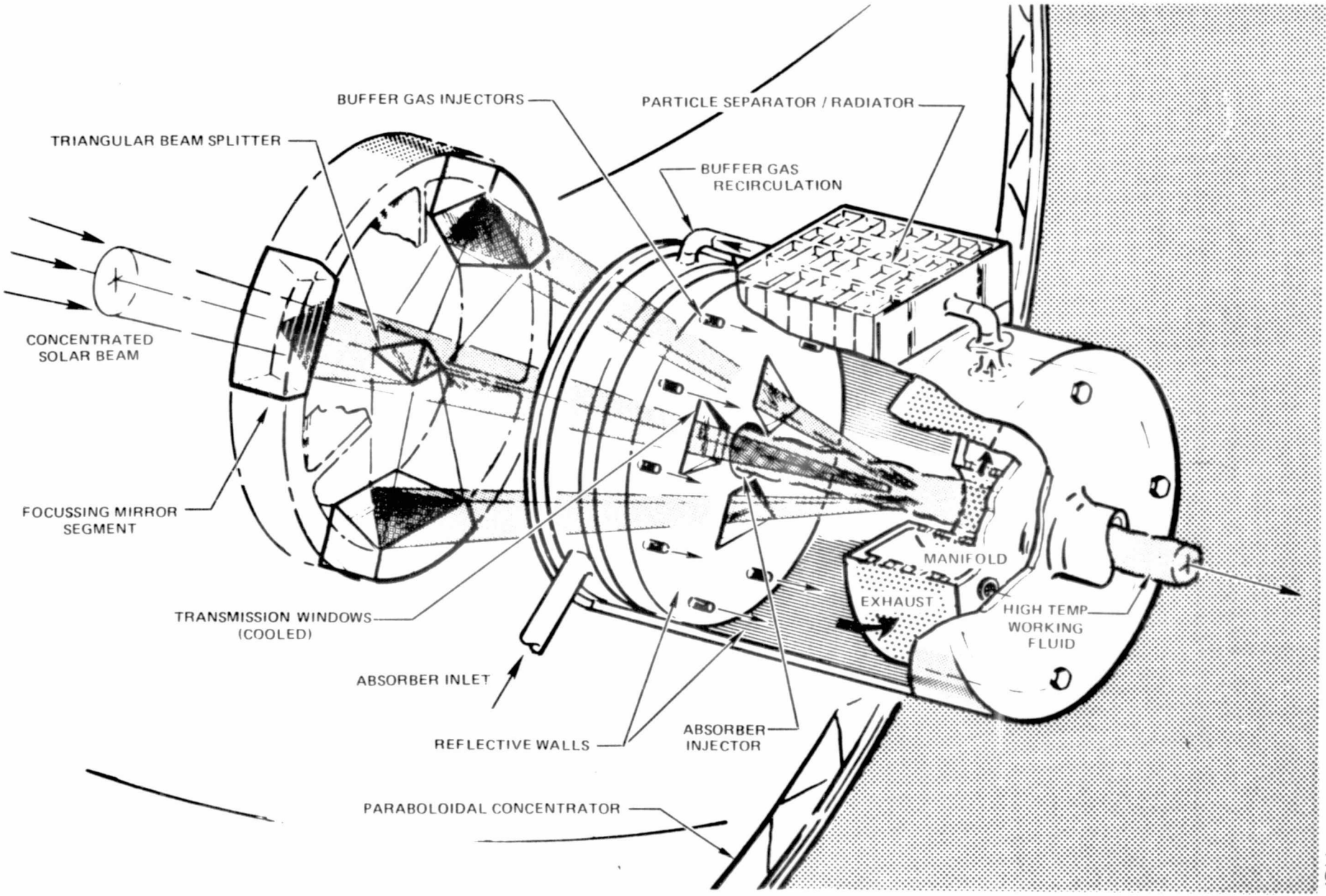

R79-914392

FIG. 1

79-02-293-1

PARABOLOIDAL COLLECTOR MODEL

SOLAR ANGULAR DIAMETER, α = 0.931 mRAD

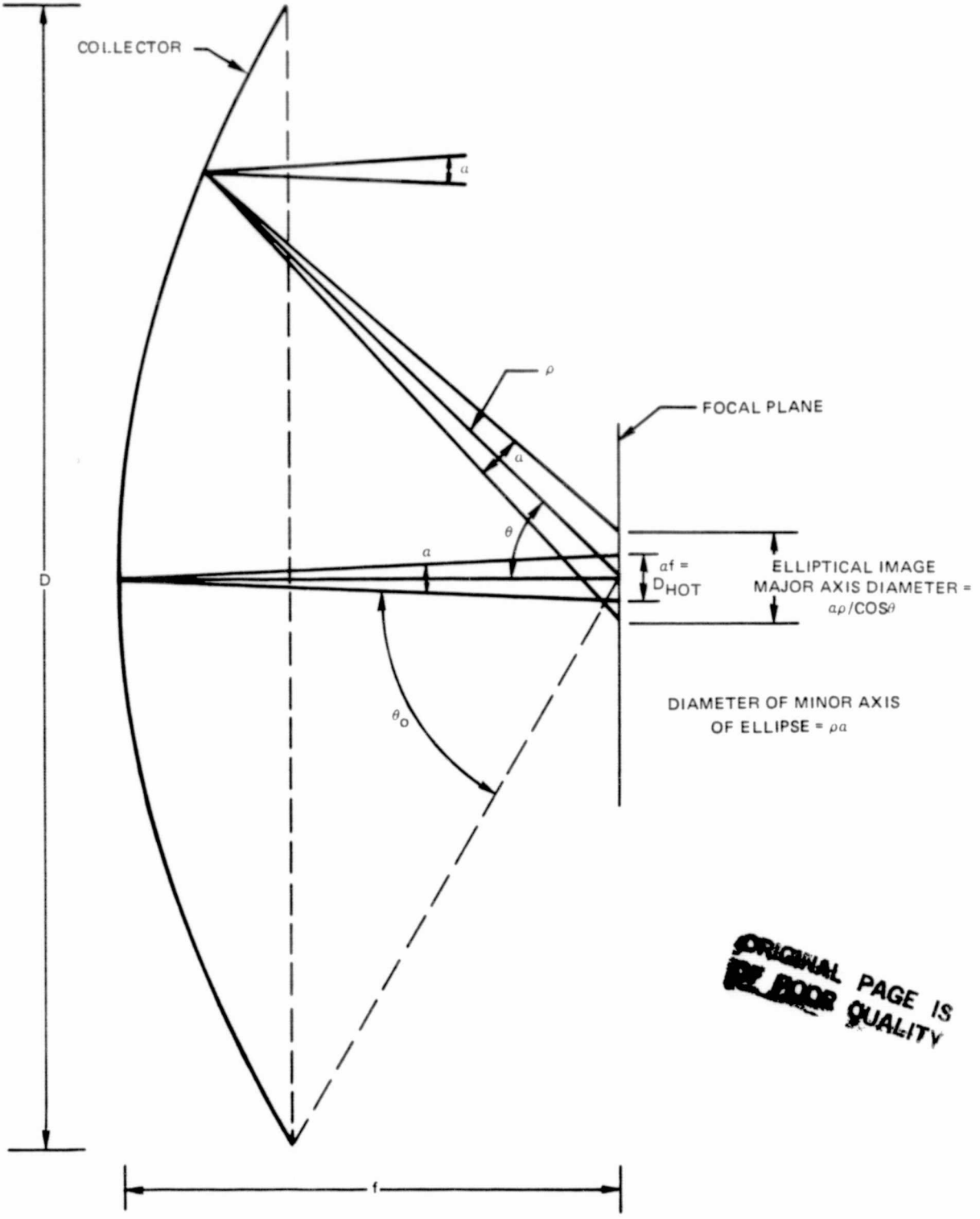

79–02–147–1

FIG. 3

VARIATION OF HOT SPOT POWER WITH PARABOLOID RIM ANGLE

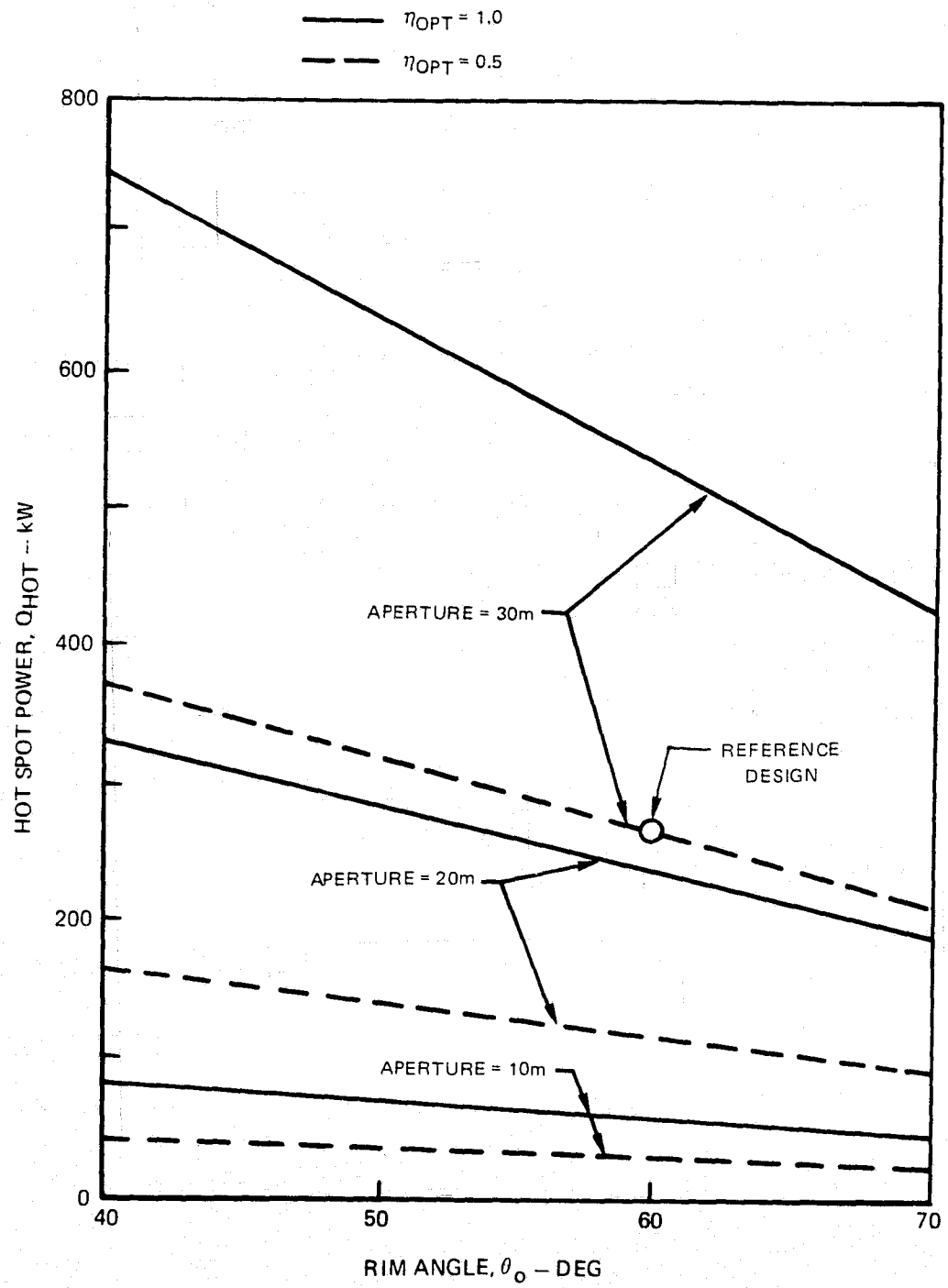

78–10–168–1

FIG. 4

VARIATION OF PERFORMANCE CHARACTERISTICS WITH RIM ANGLE FOR PARABOLOID COLLECTOR

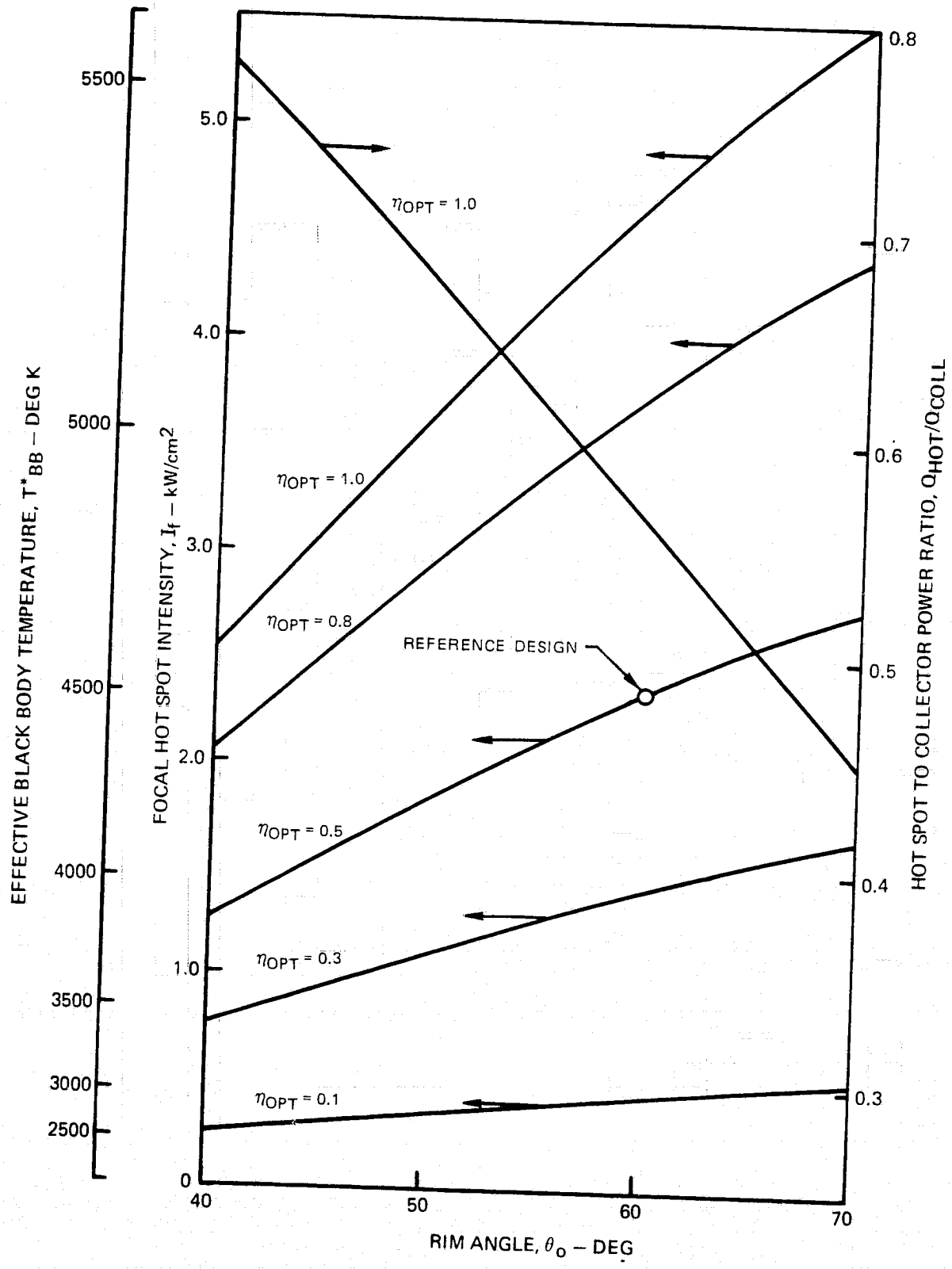

78–10–168–2

VARIATION IN FOCAL PLANE HOT SPOT DIAMETER WITH COLLECTOR GEOMETRY

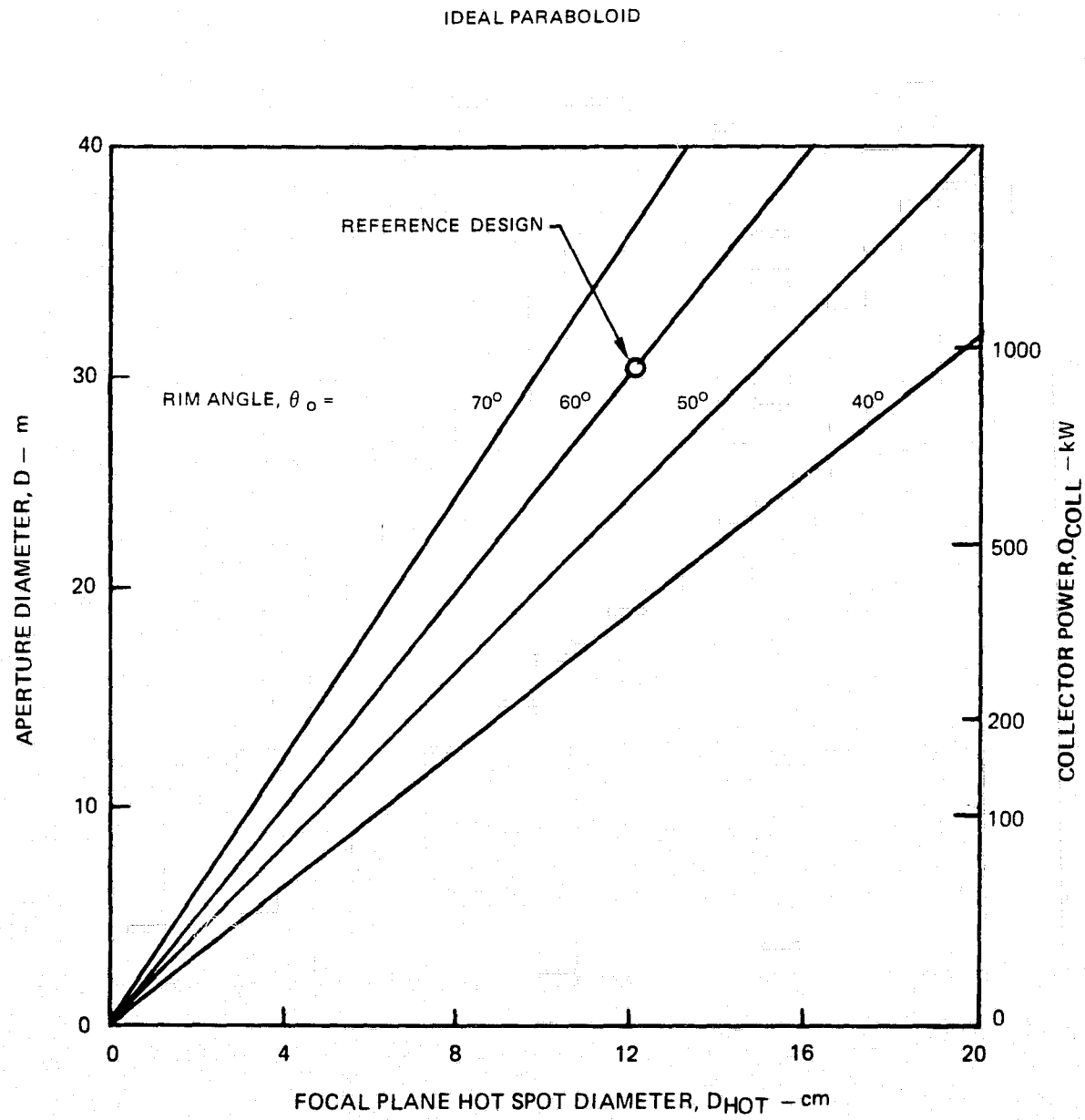

78-11-77-1

SOLAR FRACTIONAL FLUX AND SPECTRAL ABSORPTION CROSS–SECTION FOR A GAS SUSPENSION OF 0.2 MICRON DIAMETER CARBON PARTICLES

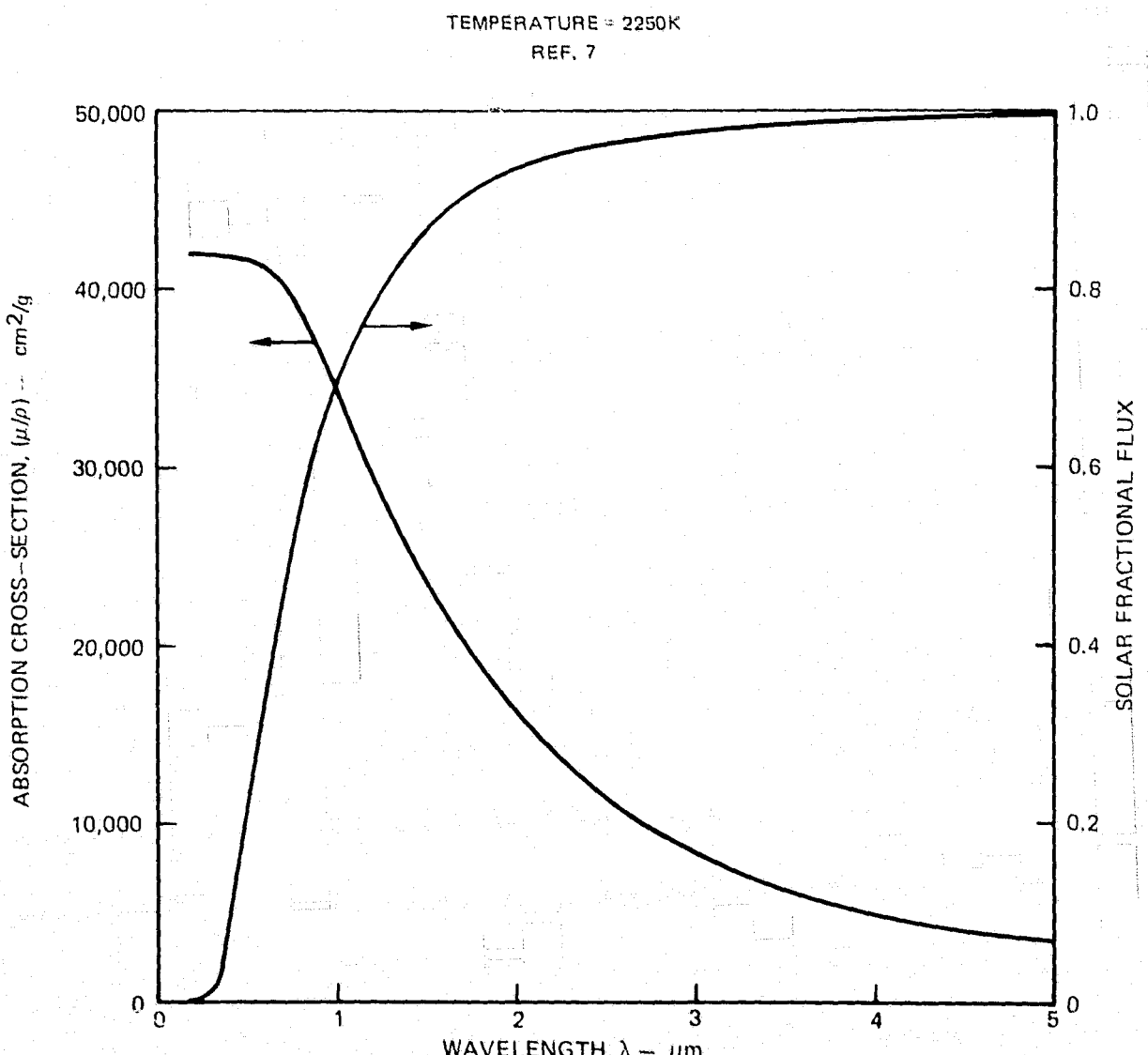

79–02–172–1

VARIATION OF VOLUMETRIC ENERGY DEPOSITION WITH RADIUS FOR A GAS SUSPENSION OF 0.2 MICRON DIAMETER CARBON PARTICLES

INCIDENT FLUX = 2.335 kW/cm^2
ABSORBER LENGTH = 12.09 cm
CARBON SEED DENSITY = 3.65 μg/cm^3
ABSORBER RADIUS = 6.045 cm
ALUMINUM REFLECTIVE WALLS

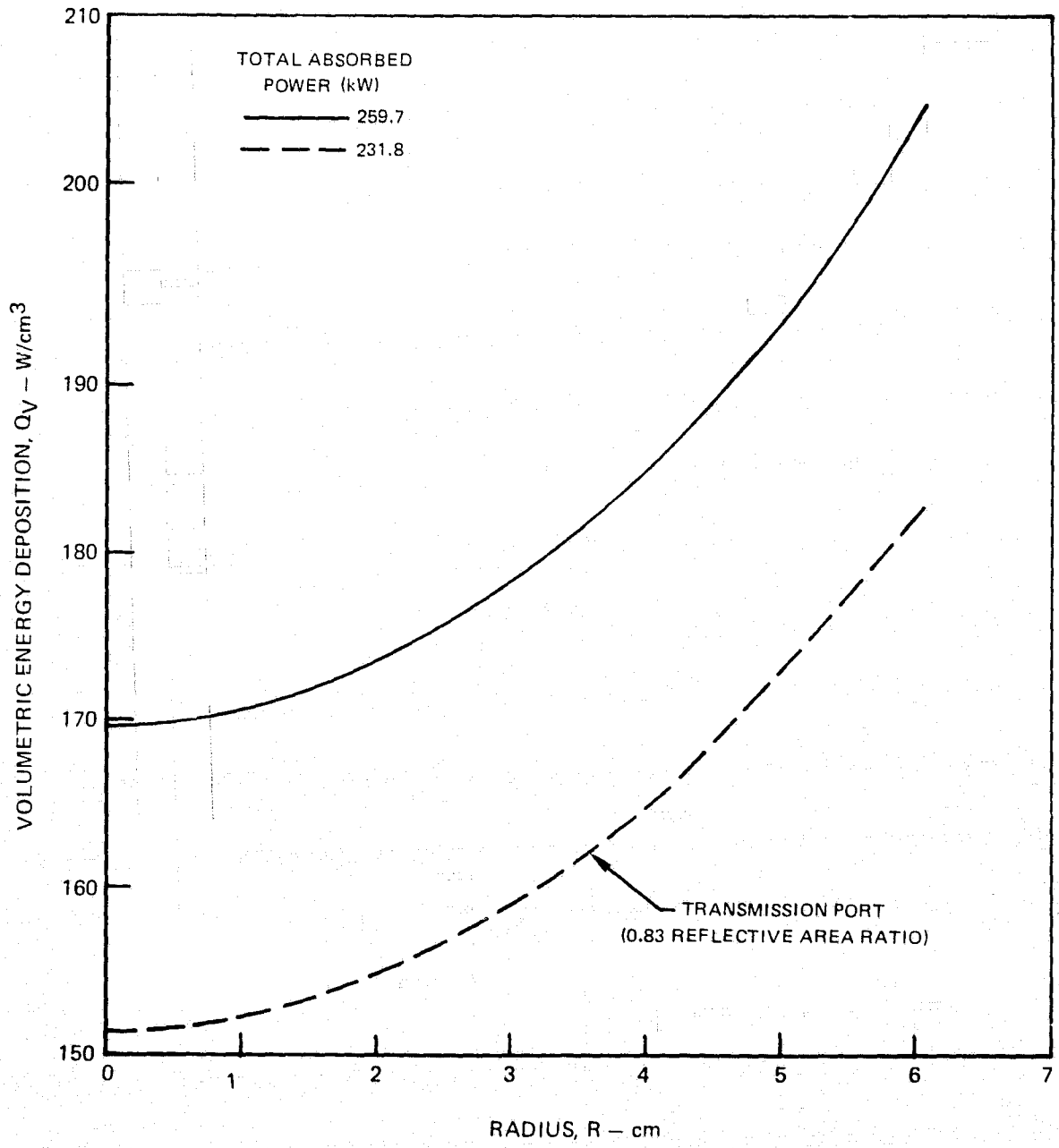

CALCULATED VARIATION OF ALUMINUM REFLECTIVITY WITH WAVELENGTH FOR SEVERAL ANGLES OF INCIDENCE

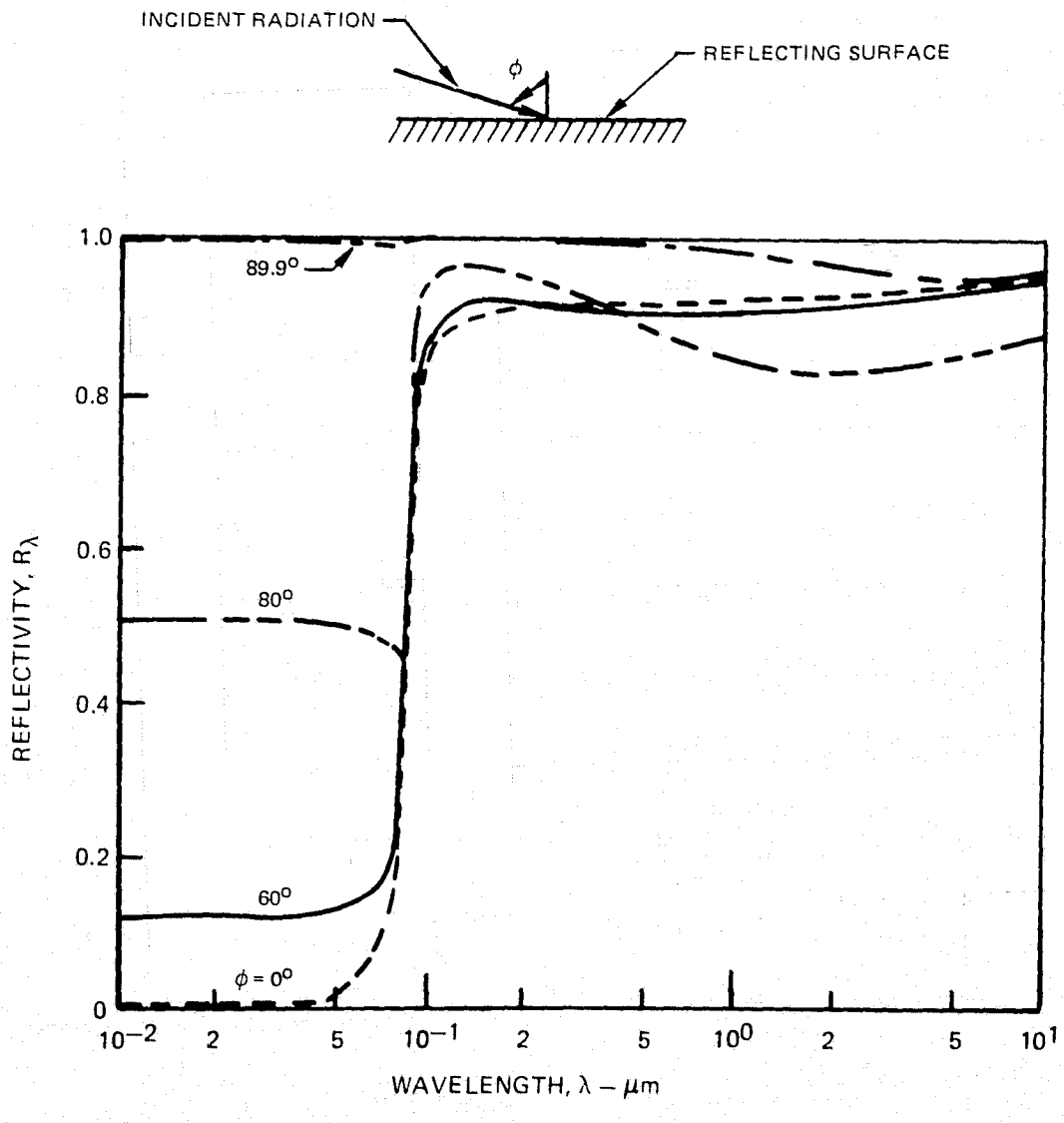

SPECTRAL VARIATION OF INCIDENT AND ABSORBED ENERGY FRACTIONS

CARBON PARTICLE DIAMETER = 0.2 MICRONS
CARBON SEED DENSITY = 3.65 $\mu g/cm^3$
ABSORBER DIAMETER = 12.09 cm

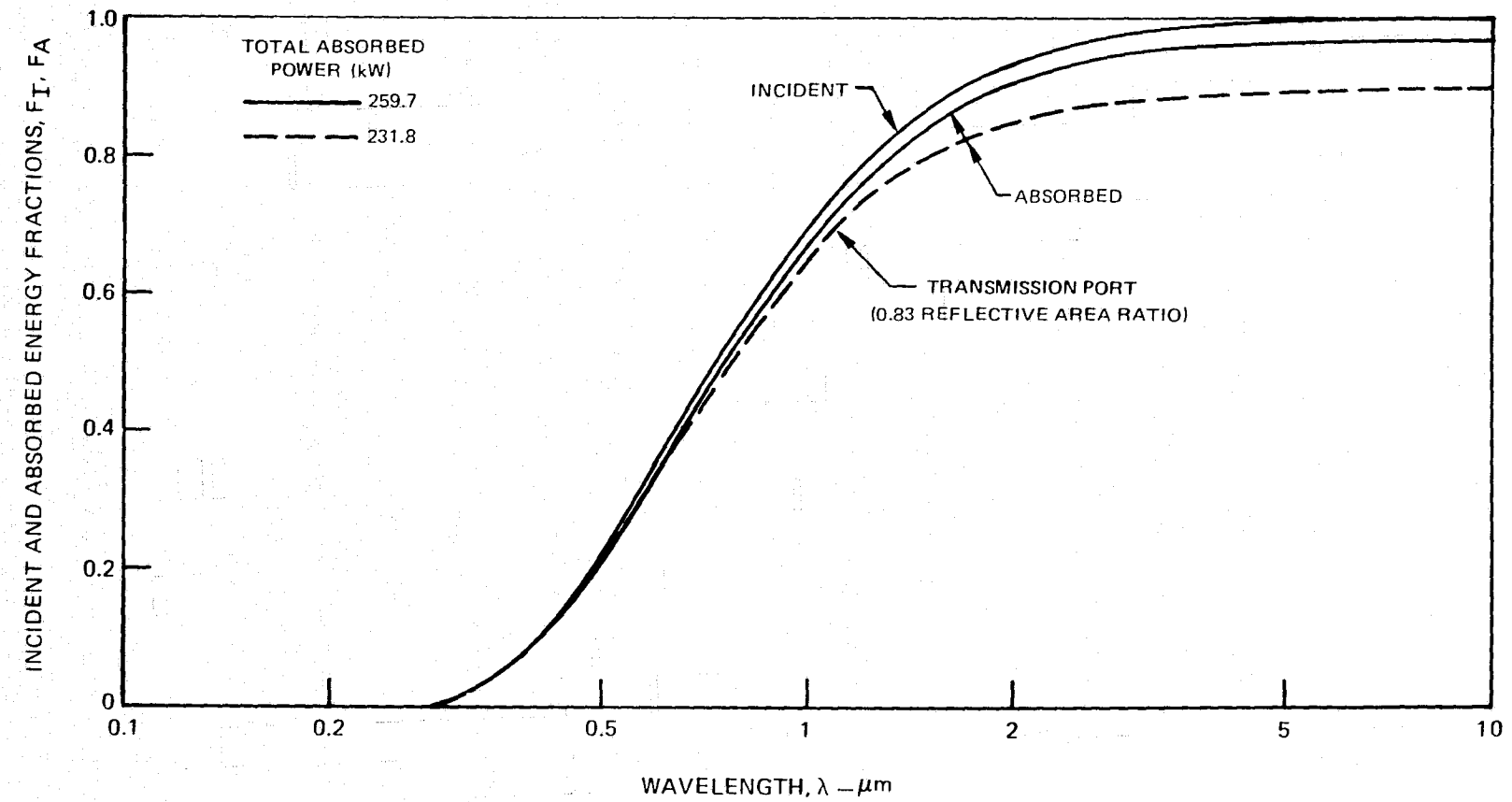

VARIATION OF TEMPERATURE WITH RADIUS FOR 0.2 MICRON DIAMETER CARBON PARTICLES IN ARGON

TOTAL PRESSURE = 10 ATM
TOTAL ABSORBED POWER = 259.7 kW
ABSORBER LENGTH = 12.09 cm
INJECTION TEMPERATURE = 300K
CARBON DENSITY = 3.65 $\mu g/cm^3$
FLOW RATE = 588 g/s
ABSORBER REGION POWER = 181.1 kW
BUFFER REGION POWER = 78.6 kW

TEMPERATURE AT EXIT OF CYLINDRICAL HEATING VOLUME

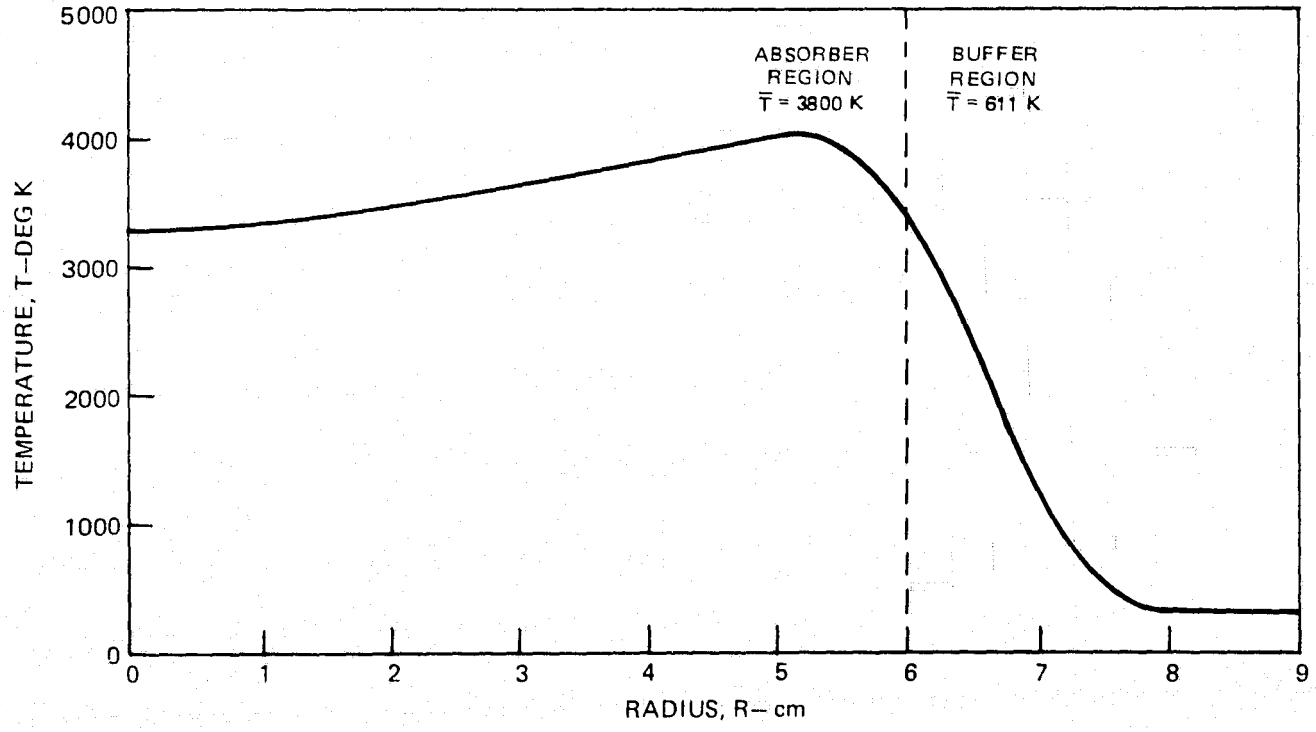

78–12–24–3

VARIATION OF INTEGRATED WEIGHT FLOW AND VELOCITY WITH RADIUS FOR 0.2 MICRON DIAMETER CARBON PARTICLES IN ARGON

TOTAL PRESSURE = 10 ATM

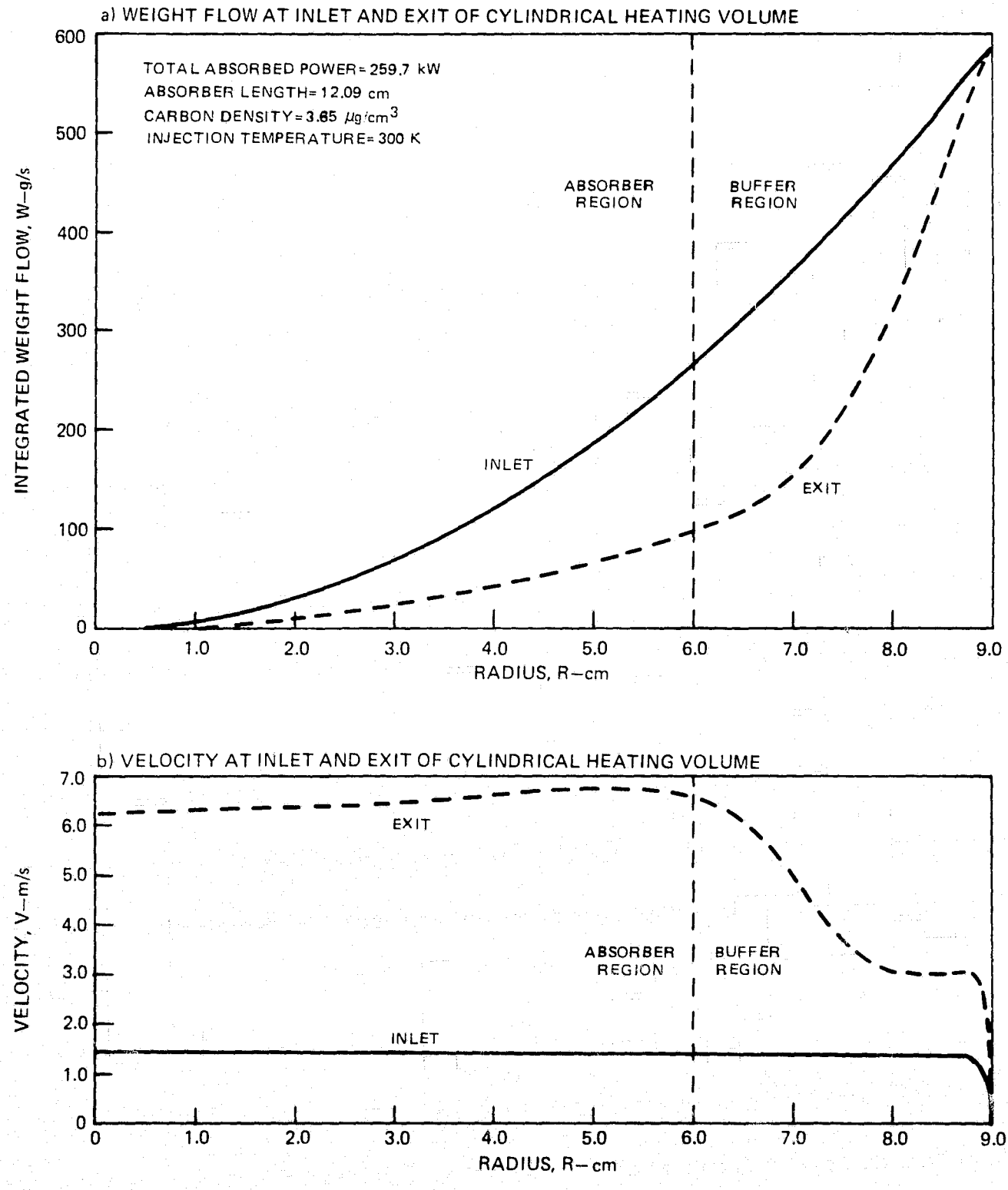

78-12-24-4

FIG. 12

COMPOSITION OF CESIUM AS A FUNCTION OF TEMPERATURE FOR VARIOUS TOTAL PRESSURE

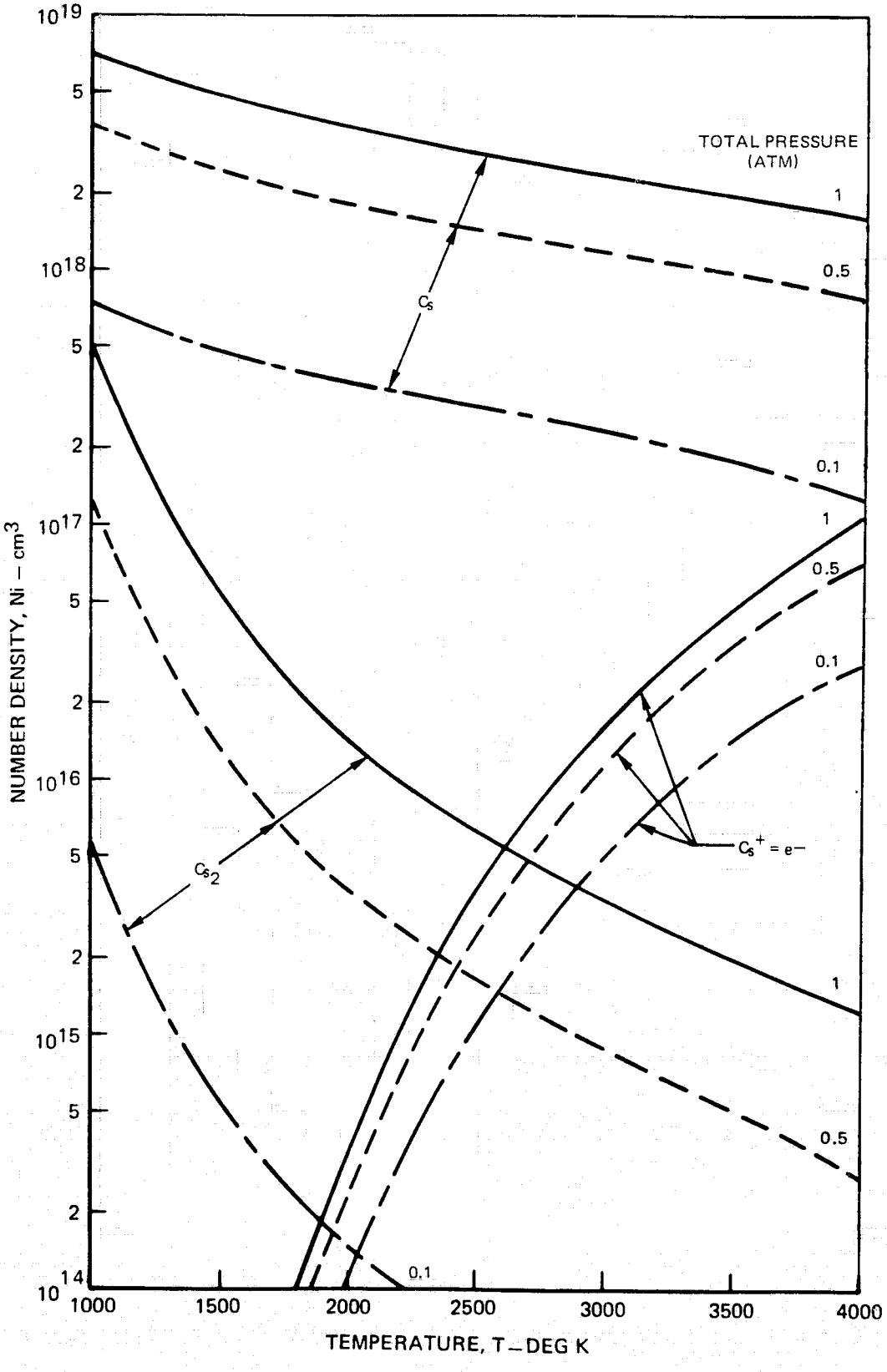

79–02–147–2

RELATIVE POPULATION OF CESIUM ATOMS IN LOW–LYING EXCITED STATES

TERM DESIGNATION	J	ENERGY cm^{-1}	BOUND–FREE THRESHOLD Å
$6p^2P^0$	1/2 3/2	11178.2 11732.4	4944 5083
$5d^2D$	3/2 5/2	14499.5 14597.1	5915 5949
$7s^2S$	1/2	18535.5	7769
$7p^2P^0$	1/2 3/2	21765.7 21946.7	10372 10571

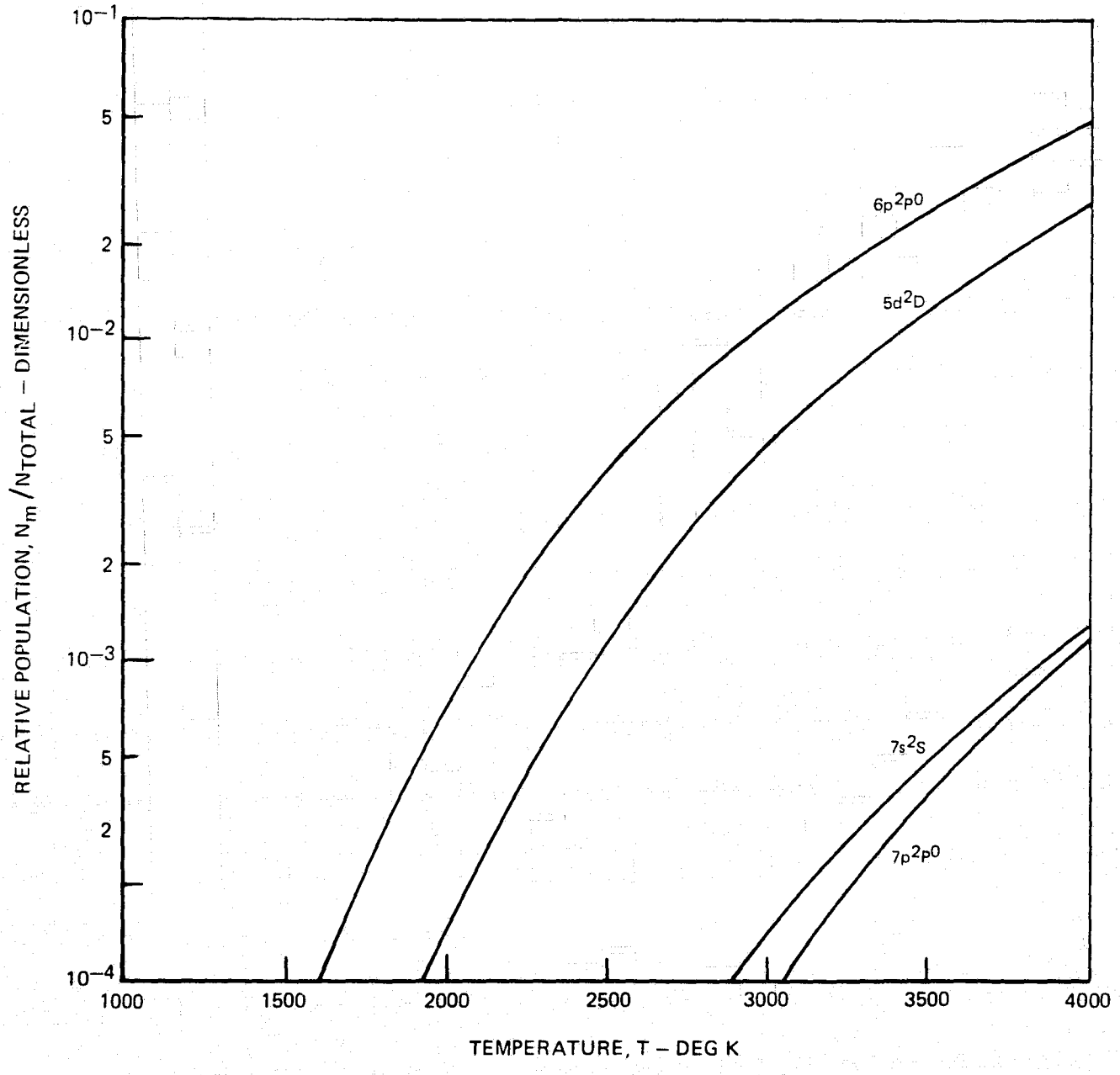

78–11–93–2

VARIATION OF CESIUM VAPOR SPECTRAL ABSORPTION COEFFICIENT AT 0.1, 0.5 AND 1.0 ATM

TEMPERATURE = 300K

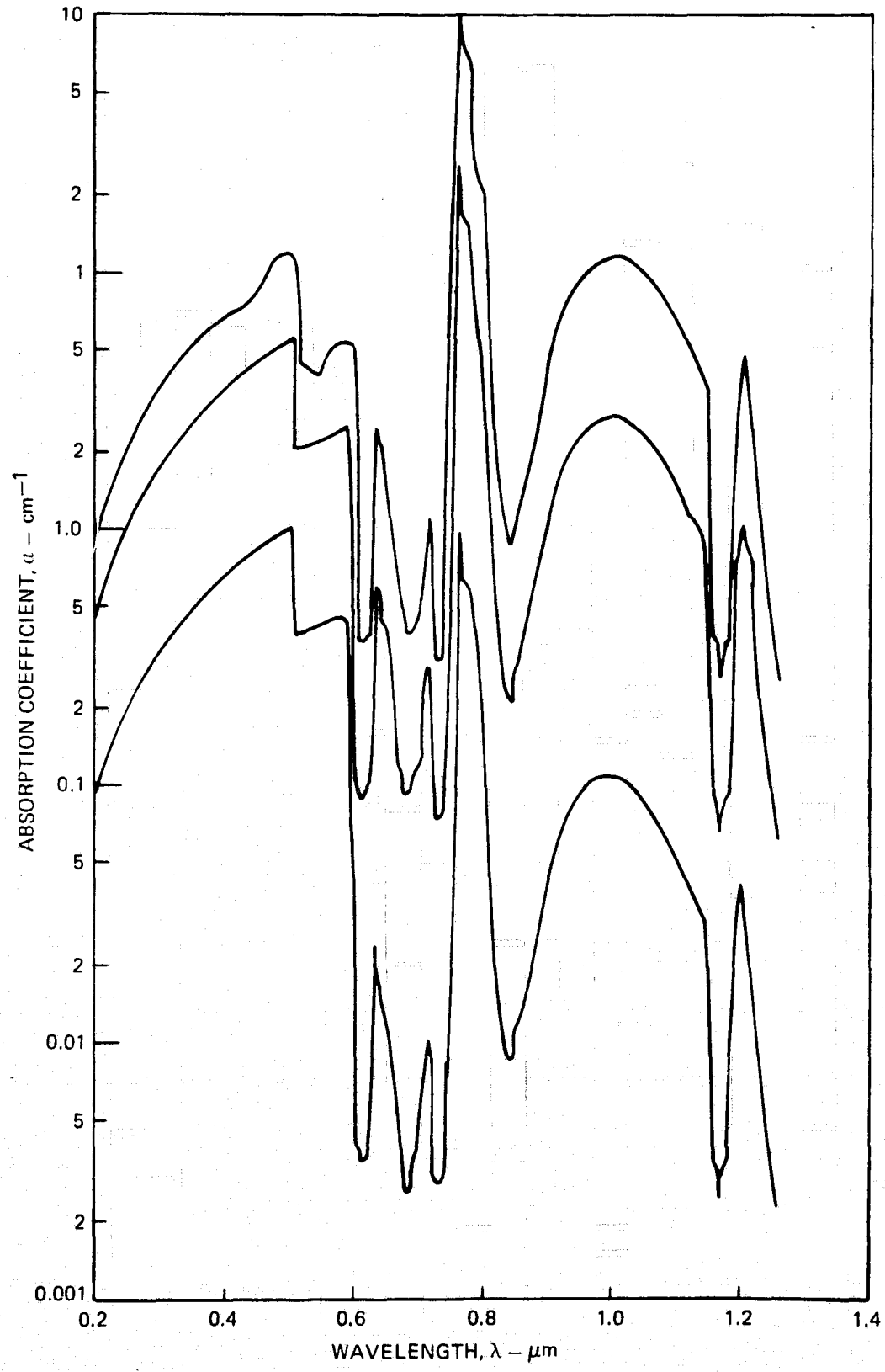

79–02–77–2

FIG. 15

VARIATION OF VOLUMETRIC ENERGY DEPOSITION WITH RADIUS FOR CESIUM VAPOR PRESSURE OF 0.1,0.5, AND 1.0 ATM

INCIDENT CONCENTRATED SOLAR FLUX = 2.335 kW/cm^2

ABSORBER LENGTH = 12.09 cm

ALUMINUM REFLECTIVE WALLS

INCIDENT POWER = 268.1 kW

PRESSURE P_{CESIUM} (ATM)	POWER ABSORBED Q_{ABS} (kW)
1.0	209.2
0.5	192.2
0.1	118.4

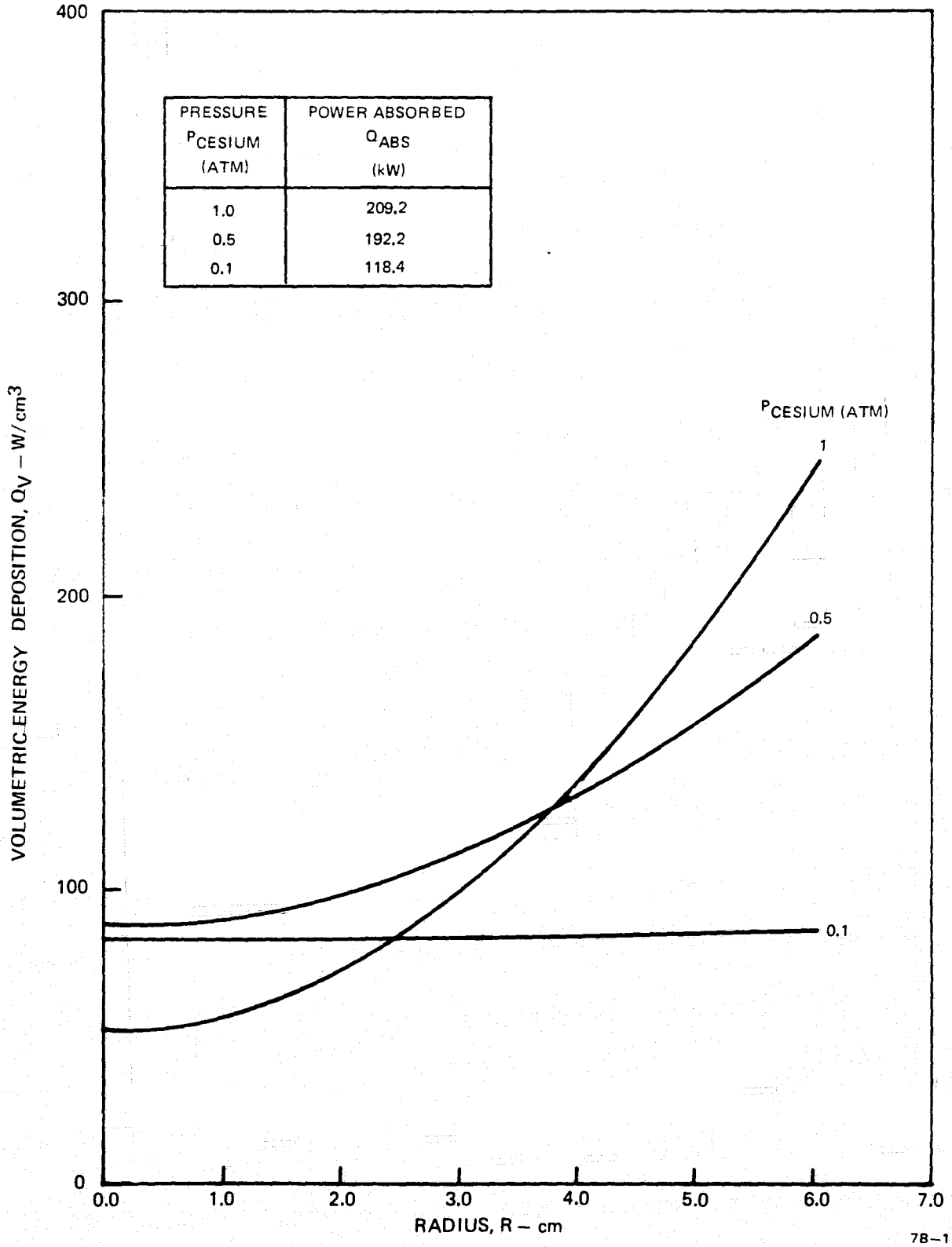

78-11-77-2

SPECTRAL VARIATION OF INCIDENT AND ABSORBED ENERGY FRACTIONS

INCIDENT CONCENTRATED SOLAR FLUX = 2.335 kW/cm^2
ABSORBER LENGTH = 12.09 cm
ALUMINUM REFLECTIVE WALLS
INCIDENT POWER = 268.1 kW

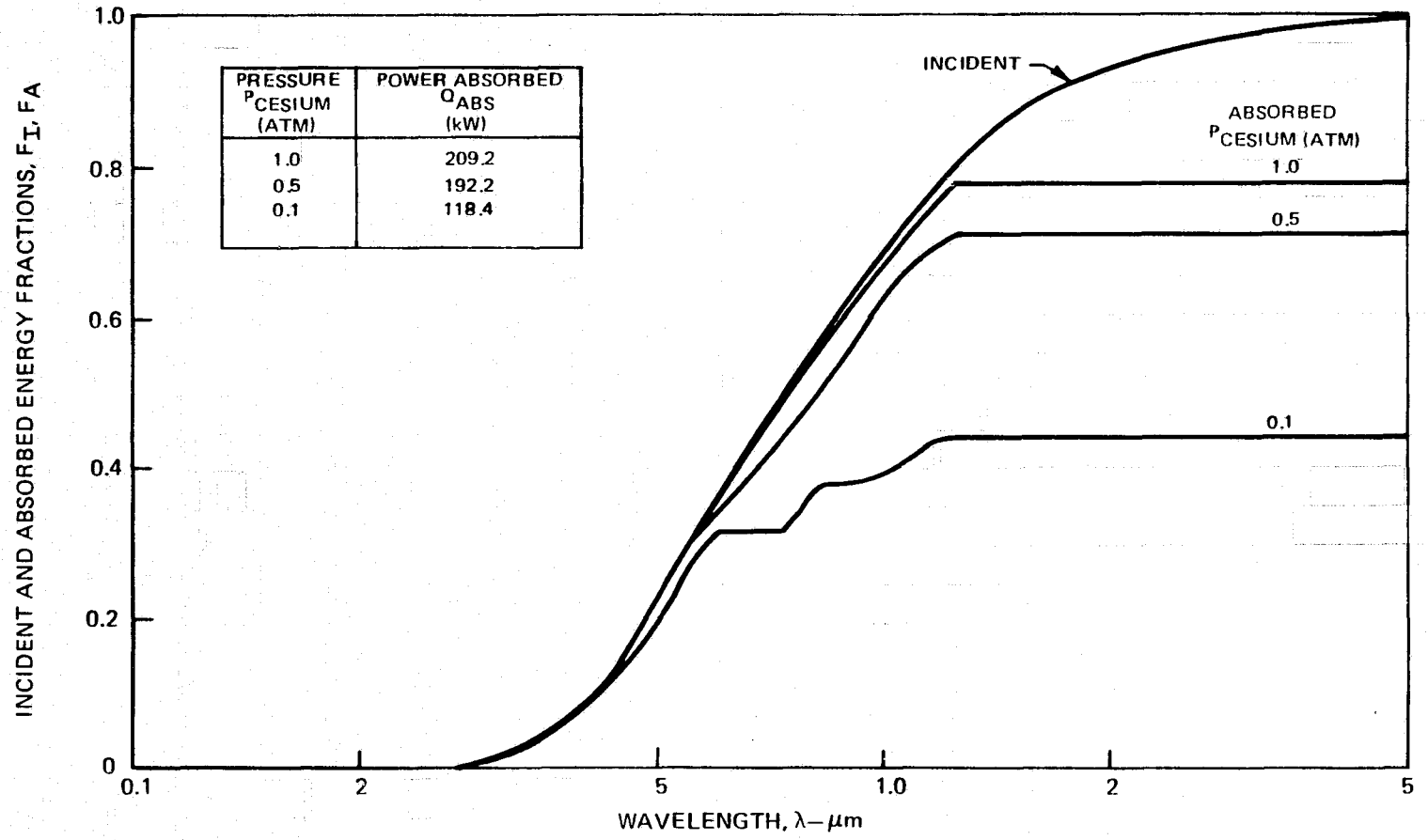

VARIATION OF TEMPERATURE WITH RADIUS FOR A 0.5 ATM PRESSURE CESIUM VAPOR ABSORBER IN ARGON

TOTAL WEIGHT FLOW = 403 g/s
TOTAL ABSORBED POWER = 192.2 kW
INJECTION TEMPERATURE = 900 K
CENTERLINE INJECTION VELOCITY = 2.83 m/s
ABSORBER LENGTH = 12.09 cm

TEMPERATURE AT EXIT OF CYLINDRICAL HEATING VOLUME

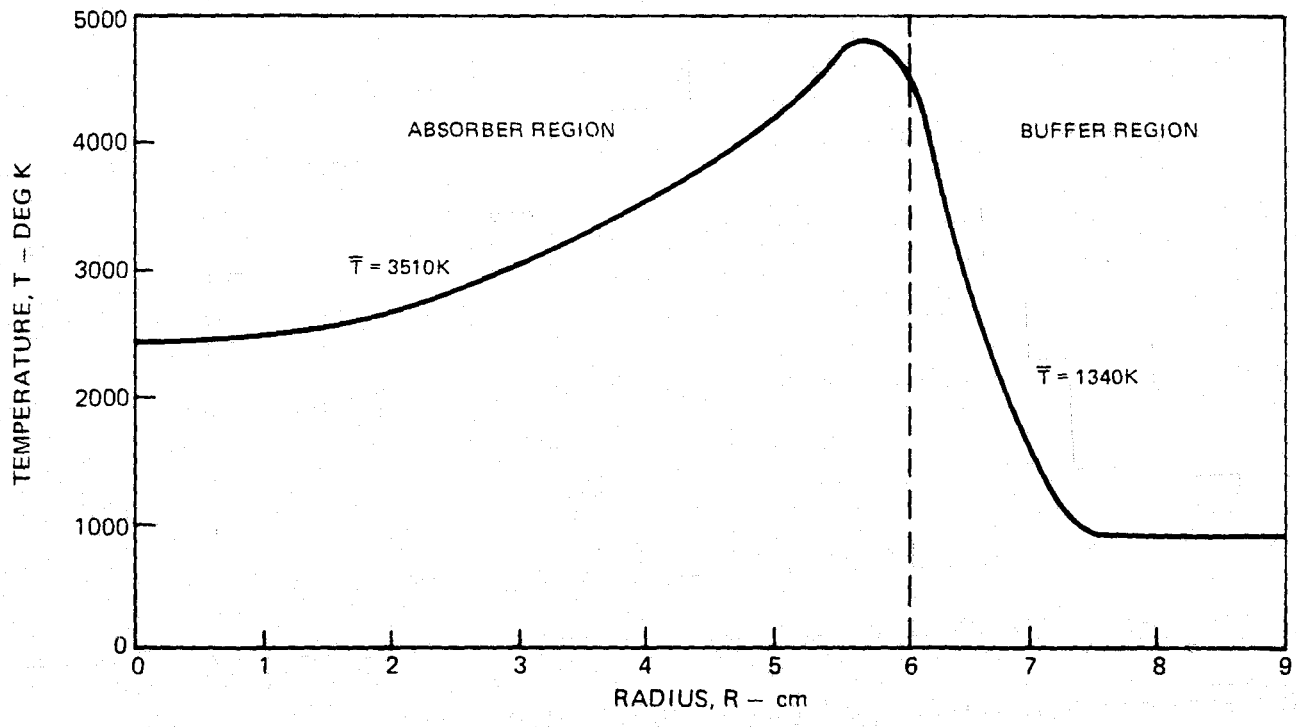

79–01–88–2

VARIATION OF INTEGRATED WEIGHT FLOW AND VELOCITY WITH RADIUS FOR A 0.5 ATM PRESSURE CESIUM VAPOR ABSORBER IN ARGON

TOTAL PRESSURE = 10 ATM
TOTAL ABSORBED POWER = 192.2 kW
INJECTION TEMPERATURE = 900 K
ABSORBER LENGTH = 12.09 cm

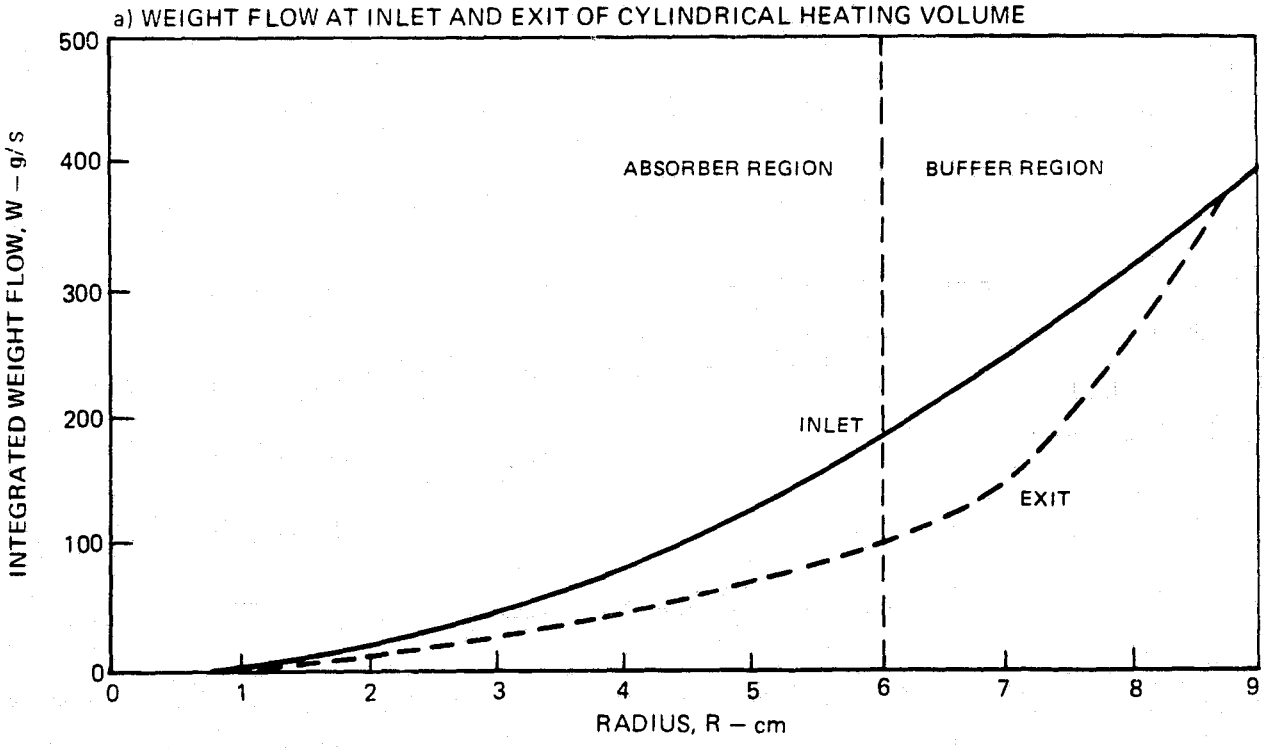

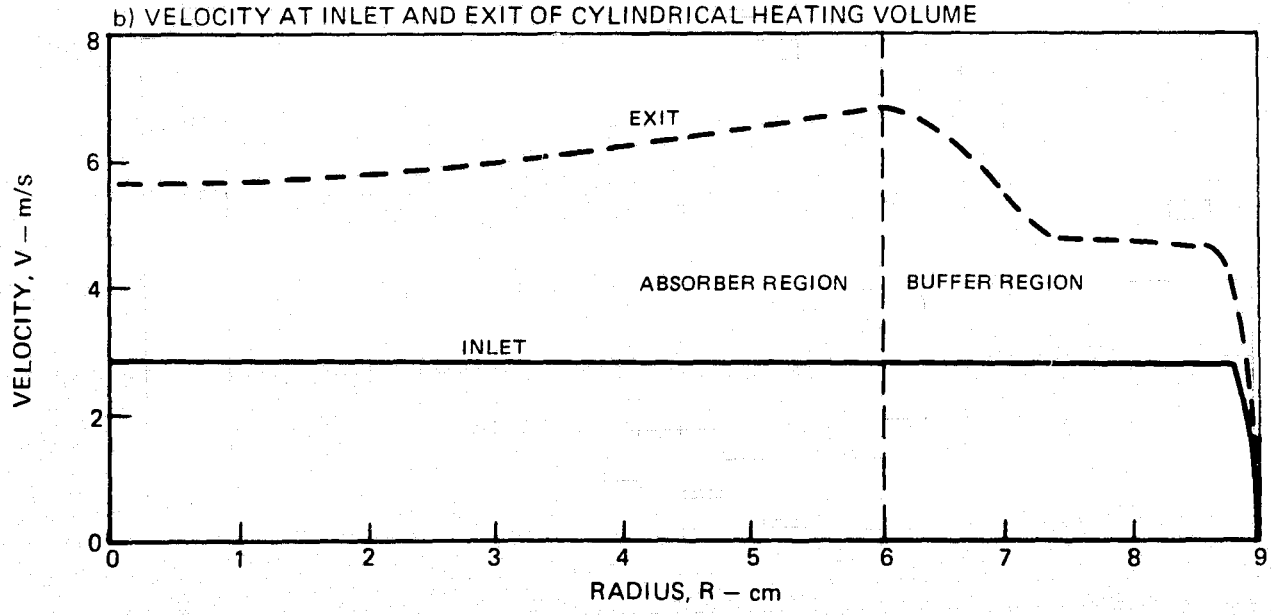

79–01–88–1

VARIATION OF NET RADIATED FLUX AT OUTER CYLINDRICAL SURFACE OF ABSORBER WITH MAXIMUM EFFECTIVE RADIATING TEMPERATURE

ASSUMES SOLAR IMAGE FLUX IS UNIFORMLY DISTRIBUTED AROUND CYLINDRICAL ABSORBER SURFACE

SOLAR IMAGE DIAMETER = 12.09 cm
CYLINDER HEIGHT = 12.09 cm
ALUMINUM REFLECTIVITY = 0.92
ALUMINUM REFLECTIVE AREA FRACTION = 0.83
TRANSPARENT AREA FRACTION = 0.17

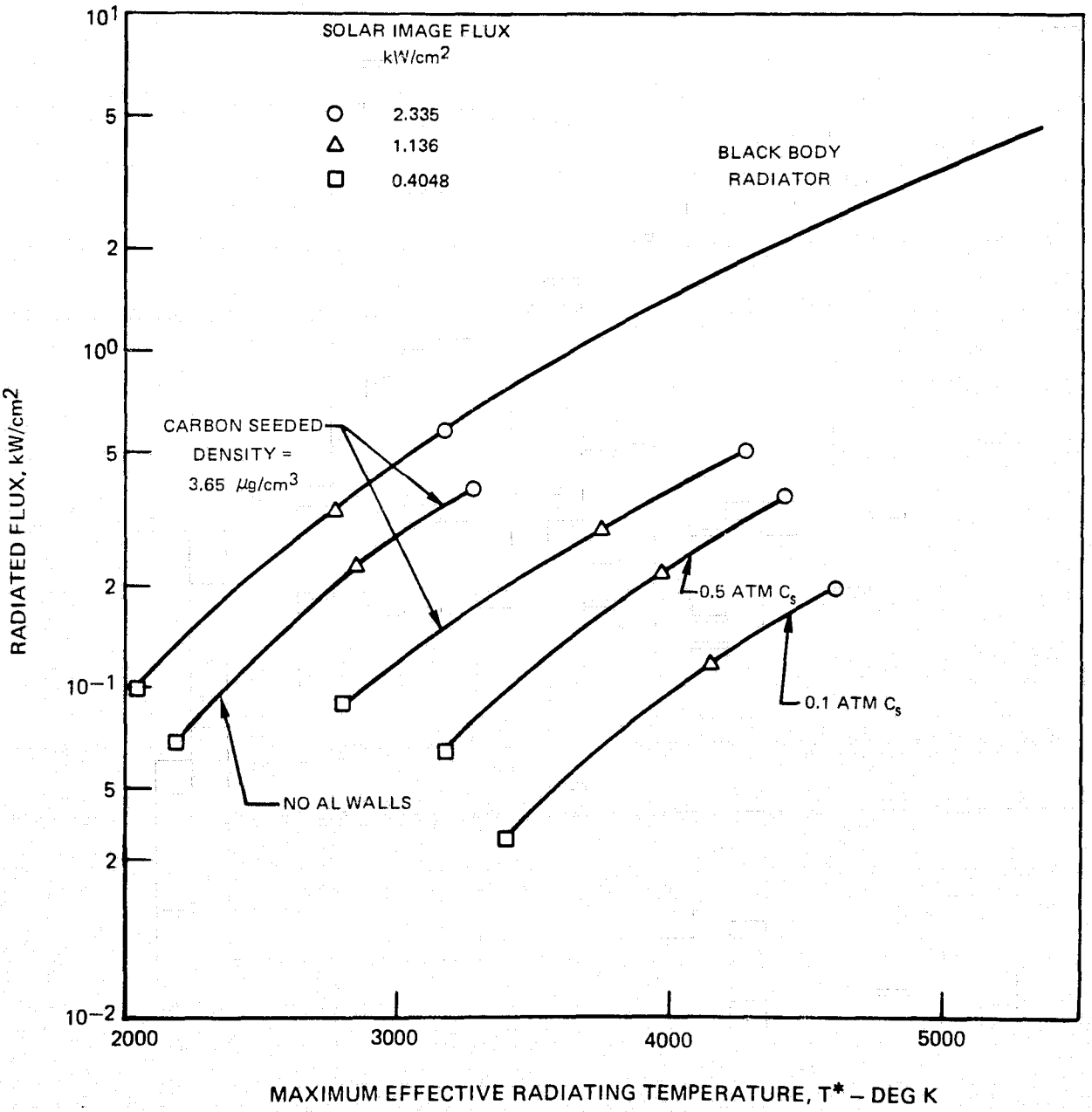

79–02–147–3

BRAYTON CYCLE FLOW SCHEMATIC FOR CARBON PARTICLE SEEDED PLASMA

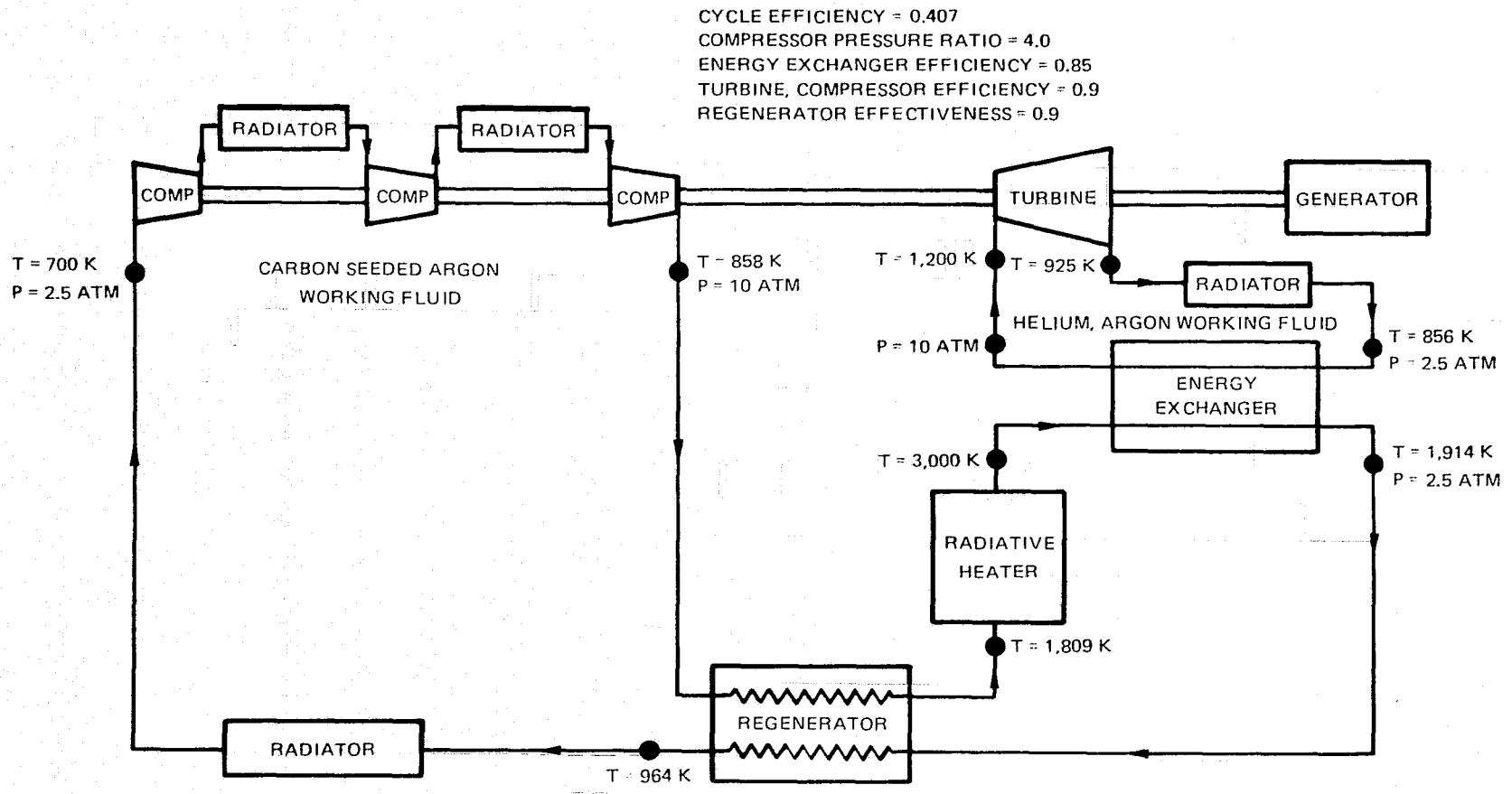

VARIATION OF BRAYTON CYCLE EFFICIENCY WITH PRESSURE RATIO FOR CARBON SEEDED ARGON WORKING FLUID AND A CYCLE REJECTION TEMPERATURE OF 700 K

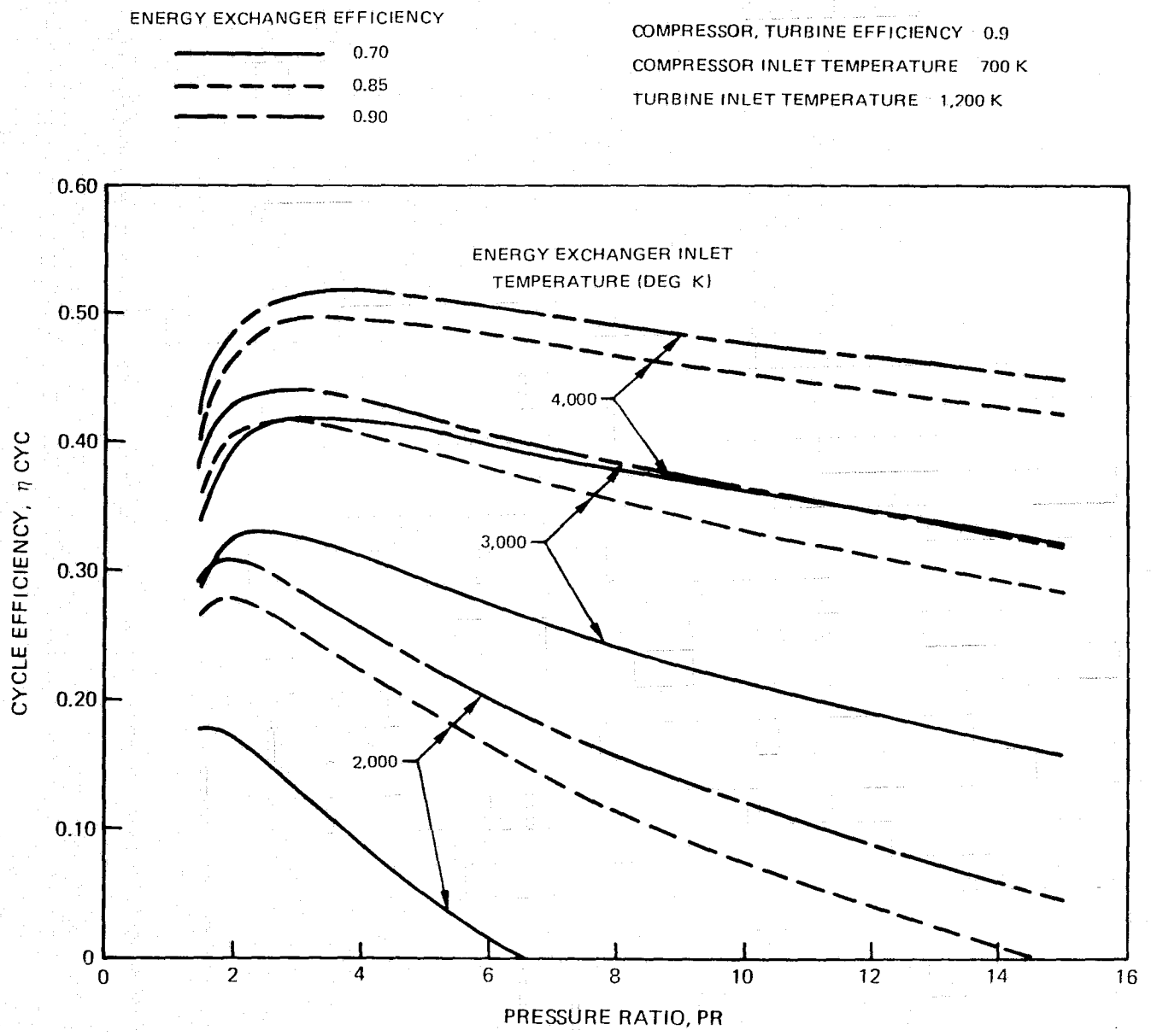

R79-914392

79-02-202-3

FIG. 21

VARIATION IN REGENERATOR INLET TEMPERATURE WITH PRESSURE RATIO FOR CARBON PARTICLE SUSPENSION IN ARGON WORKING FLUID

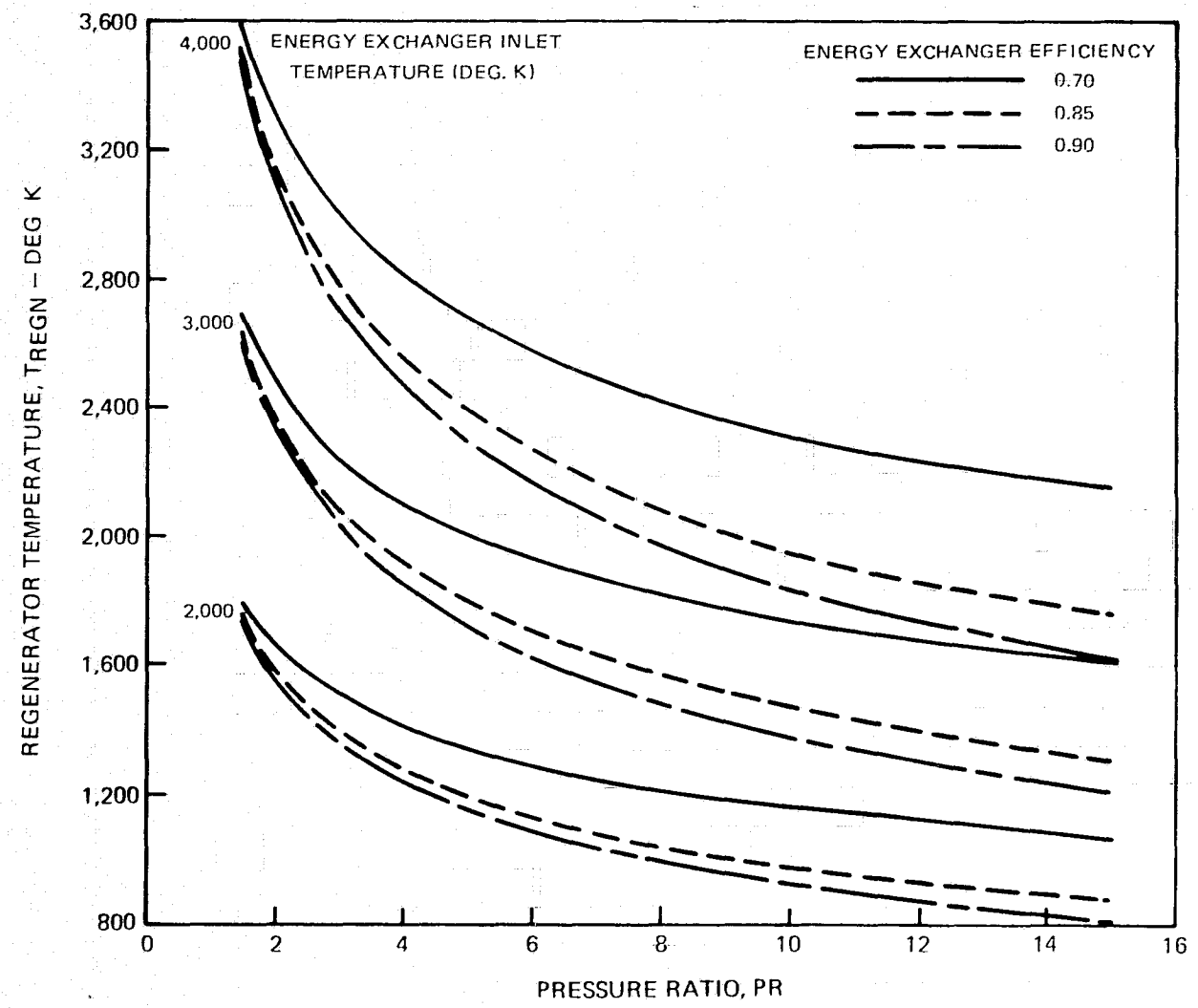

VARIATION OF BRAYTON CYCLE EFFICIENCY WITH PRESSURE RATIO FOR CARBON SEEDED ARGON WORKING FLUID FOR A CYCLE REJECTION TEMPERATURE OF 320K

COMPRESSOR, TURBINE EFFICIENCY = 0.9

TURBINE INLET TEMPERATURE = 1200K

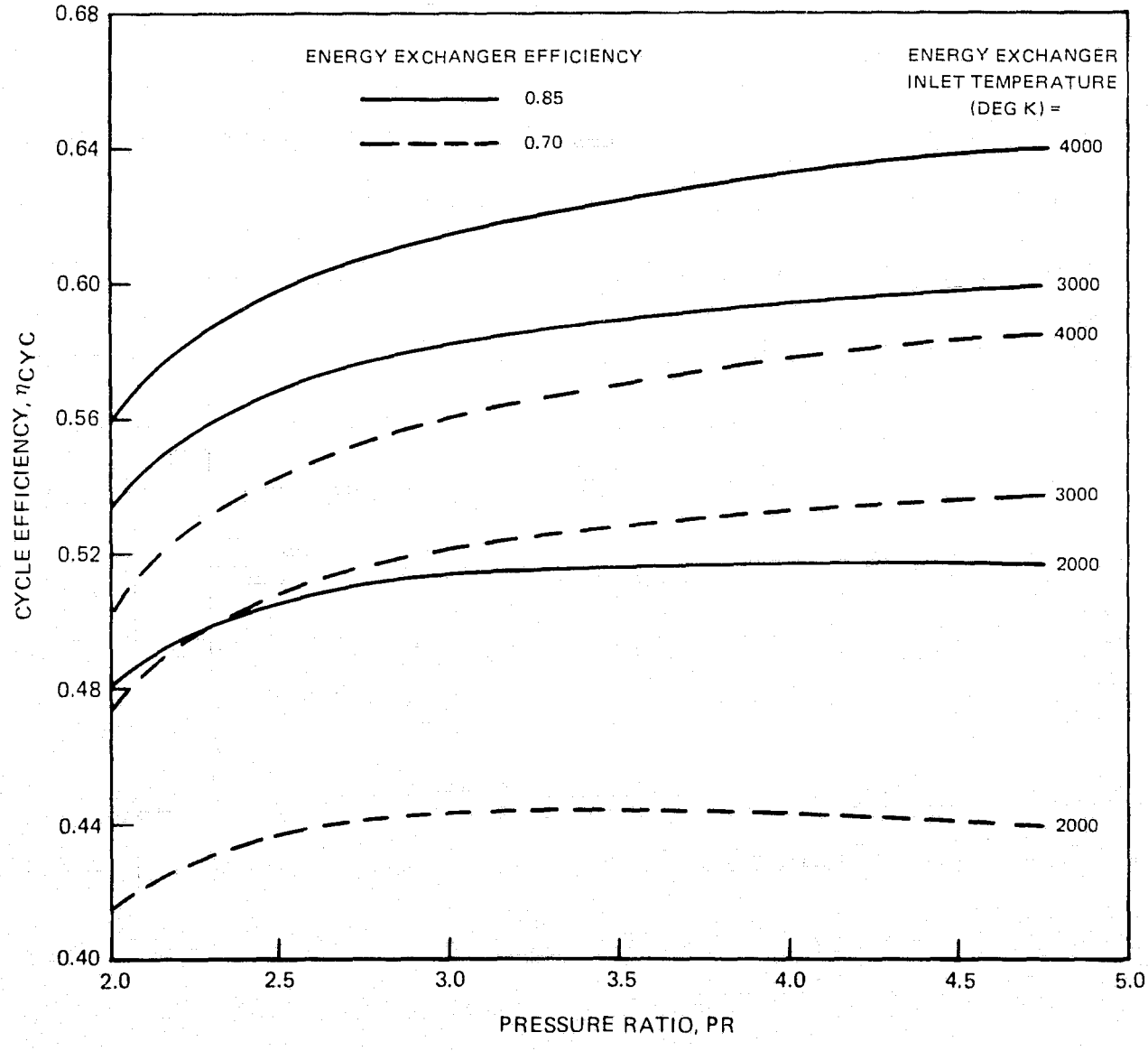

79–02–77–7

VARIATION IN BRAYTON CYCLE EFFICIENCY WITH PRESSURE RATIO FOR 0.5 ATM CESIUM VAPOR IN ARGON WORKING FLUID FOR A CYCLE TEMPERATURE OF 900K

COMPRESSOR, TURBINE EFFICIENCY = 0.9
TURBINE INLET TEMPERATURE = 1200K